Tactile Sensor Design Optimization for Footwear Applications

From Piezoresistive Elastomer to Hall-Effect Integrated Sensing Methods

by
Ann (Annie) Chen

Submitted to the Department of Mechanical Engineering
in Partial Fulfillment of the Requirements for the Degree of

Bachelor of Science in Mechanical Engineering

at the

MASSACHUSETTS INSTITUTE OF TECHNOLOGY

June 2018

© 2018 Ann (Annie) Chen. All rights reserved.

The author hereby grants to MIT permission to reproduce and to
distribute publicly paper and electronic copies of this thesis document
in whole or in part in any medium now known or hereafter created.

Signature redacted

Signature of Author: .....

Department of Mechanical Engineering

Signature redacted

Certified by: .....

Sangbae Kim
Associate Professor of Mechanical Engineering
Thesis Supervisor

Signature redacted

Certified by: .....

Rohit Karnik
Associate Professor of Mechanical Engineering
Undergraduate Officer

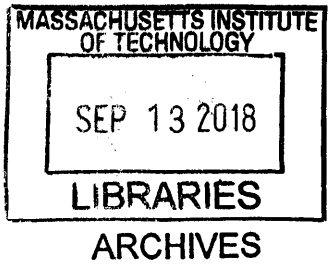

MIT Libraries

77 Massachusetts Avenue
Cambridge, MA 02139
http://libraries.mit.edu/ask

DISCLAIMER NOTICE

Due to the condition of the original material, there are unavoidable flaws in this reproduction. We have made every effort possible to provide you with the best copy available.

Thank you.

The images contained in this document are of the best quality available.

Tactile Sensor Design Optimization for Footwear Applications

From Piezoresistive Elastomer to Hall-Effect Integrated Sensing Methods

by
Ann (Annie) Chen

Submitted to the Department of Mechanical Engineering May 9, 2018
in Partial Fulfillment of the Requirements for the Degree of
Bachelor of Science in Mechanical Engineering

Abstract

Our ability to move across various terrains depends heavily on the mechanical interactions between our feet and the external environment. Understanding how to best replicate mechanoreceptors in feet can lead to major improvements in plantar sensing for athletic performance analysis and medical devices. However, current plantar sensing technologies are unable to meet the associated demands for accuracy, sensitivity, and durability. In addition, current sensors are also unable to withstand the large impact forces and inertial noise associated with human locomotion.

To address this issue, this thesis investigates alternative designs for a tactile force sensors that are largely inspired by mechanoreceptors found in human skin. Two different sensing methodologies will be analyzed: piezoresistive elastomer and Hall-effect integration. The piezoresistive elastomer method will involve testing mixtures of urethane or silicone rubbers with various conductive substances such as carbon black. Compressing the sensors at various forces will correspond to lower resistance measurements as more electrical connections are made by the conductive particulates. Though these designs have high sensitivity to changes in force, the resulting data is inconsistent and slow to stabilize due to material creep. The Hall-effect integrated method will involve a magnet and four Hall-effect sensors molded in an elastomer matrix. Compressing the sensors will register different readings in each of the four embedded Hall-effect sensors which will correspond to a certain shear and deflection measurement. This sensor design shows promise as a cost-effective plantar sensor, but additional analysis is needed.

Thesis Supervisor: Sangbae Kim

Title: Associate Professor of Mechanical Engineering

Though these designs can used as general sensing approaches for other tactile force sensor designs, the specific application in mind is for integration in the soles of shoes. Specifically, these relatively thin sensors will allow for pressure distribution measurements to be done within the confines of current shoe designs. Foot pressure measurements will be able to occur real-time with minimal obstacles to the user and no longer restrict data collection to stationary force plates in lab settings. As a result, this would change the way we quantify and improve athletic performance, robotics, and medical treatments.

Thesis Supervisor: Sangbae Kim
Title: Associate Professor of Mechanical Engineering

Acknowledgements

I have received a lot of invaluable guidance and assistance on this project. I am extremely thankful for everything that everyone in the Biomimetics Robotics Lab has done to make the entire experience so rewarding. First, I would like to thank Professor Sangbae Kim and Dr. Meng Yee (Michael) Chuah for their direct assistance and involvement on this project. For the past two years, I have learned a tremendous amount under their tutelage, and for that, I am extremely appreciative. Secondly, I would also like to thank Evan Brown, Ben Katz, Juan "Sarah" Romero, Sid Trehan, and Albert Wang for helping me use the various equipment in the Biomimetics Robotics Laboratory and for their companionship throughout this process. Finally, I would like to thank my parents, Jie Chen and Ting He, my sister, Ellen Yi Chen Mazumdar, and my brother-in-law, Ani Mazumdar for their support and advice throughout my four years studying at MIT. Without any of these people, I would not be as grateful for this experience as I am today.

Contents

List of Figures

List of Tables

Chapter 1

Introduction

Humans are capable of amazing feats of balance and coordination. For activities like gymnastics or tennis, having sensory information from feet is critical for precise movements and balance correction. Being able to replicate these sensing capabilities in footpad sensors is especially useful for medical and athletic applications. In medicine, having these sensors integrated into shoes allows for constant patient monitoring for conditions like diabetes mellitus and peripheral neuropathy. In athletics, these sensors can provide real-time feedback to people looking to improve their athletic performance.

However, current tactile sensing technologies are primarily focused on replicating palmar sensing (or sensitivity in the hands) and stationary sensing methods. As a result, most current tactile sensors are designed for dextrous manipulation and fine motor control and saturate under the high impact forces involved in human locomotion. In addition, sensors like force plates and load cells, which are useful in measuring the high-magnitude footfall forces, are not small, light, or durable enough for shoe integration. They are also subject to inertial noise, which is where the mass of the sensor creates noise in the data when experiencing high velocity swings or shakes. This is especially problematic in plantar sensing where the sensor must undergo large leg swings from walking or running.

It thus becomes necessary to design an alternative tactile sensor that is able to measure large magnitude forces with good accuracy and sensitivity while also being thin and

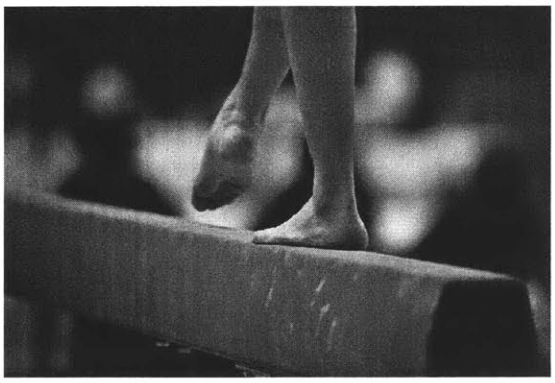

Figure 1.1: Gymnast on a Balance Beam. Gymnasts are able to use sensory information from their feet to make precise movements and aid in balance correction.

lightweight. However, not all piezoresistive elastomeric sensors and hall-effect integrated sensors are capable of meeting these requirements. The purpose of this thesis is to investigate and propose such sensor designs and augment future optimization research in plantar sensing.

1.1 Mechanoreceptors

When designing a plantar sensor for shoe integration, in addition to dimensional constraints, the sensor must also have high sensitivity, wear resistance, and robustness. The reason why these features are particularly important in plantar sensing can be found by analyzing their biological analog. The group of biological components in human skin for mechanical sensory input is called "mechanoreceptors." Mechanoreceptors allow humans to detect changes in pressure, texture, and vibration among other things. Of particular importance to this thesis is a subgroup of mechanoreceptors known as cutaneous mechanoreceptors which are specific to mechanical sensing.

There are four subcategories within this group: slow adapting type I (Merkel discs), slow adapting type II (Ruffini endings), fast adapting type I (Meissner's corpuscles), and fast adapting type II (Pascinian corpuscles). Slow adapting sensors detect maintained pressure while fast adapting sensors respond only to the stimulus' onset and offset. In other words,

slow adapting sensor are like mechanical sensors that continue sending signals under static pressure conditions while fast adapting sensors respond more to changes in pressure. Also, type I sensors have small receptive fields while type II sensors have large receptive fields, where receptive field defines the area of interest for a particular mechanoreceptor.

Initial intuition suggests that the human foot is largely comprised of SA receptors because of the importance of plantar pressure distribution information to human locomotion. However, one study found that approximately half of the mechanoreceptors in the average human foot are fast adapting type I while the remainder is evenly split among the other three types [16]. Fast adapting type I sensors are the most pressure change sensitive of the cutaneous mechanoreceptors but has one of the larger receptive fields (3–5mm in diameter) [14]. This indicates that there is a need for high dynamic sensitivity in plantar sensing to inform balance and motor control. However, because of the large receptive field, information about the spatial detail is not as crucial. In other words, detecting changes in the plantar pressure distribution field is far more important than measuring the magnitudes of pressure or irregular terrain point forces.

The same study concluded from its findings that the mechanoreceptors in the feet behave differently than those in the hands due to different receptor activation thresholds. In both fast and slow adapting cutaneous mechanoreceptors, the median activation thresholds were much higher in feet than in hands. This makes sense as feet experience larger loads more often than hands and should not saturate as quickly. This further emphasizes the importance of designing plantar specific sensors in balance and movement control. A plantar sensor must have high sensitivity for accurate readings as well as shock absorbency and durability to withstand the high loads from repeated foot strikes.

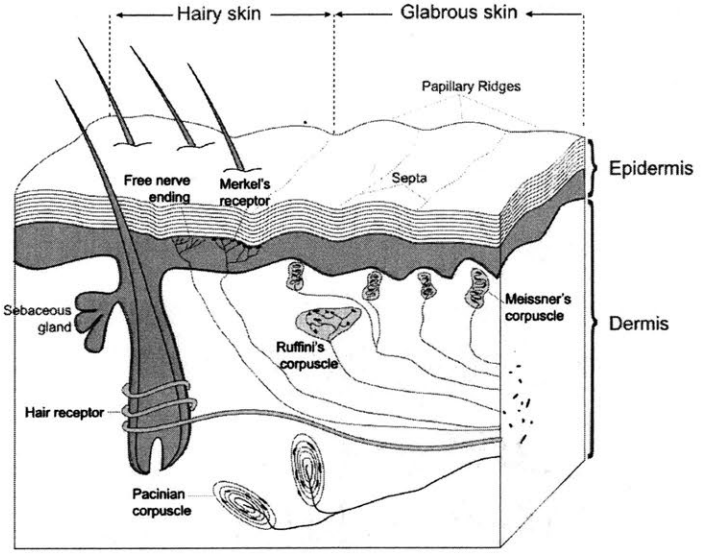

Figure 1.2: Cross-section of Human Integumentary Anatomy with Attention to Mechanoreceptors. Receptors in human skin are important for mechanical sensing. Meissner's corpuscles, which are useful for sensing changes in pressure, are especially important to characterize and replicate in plantar sensing.

1.2 Desirable Sensor Features for Athletic Performance Analysis

By 2022, the global sports footwear market is expected to reach a net worth of $89.6 billion. Nike and Adidas as well as around 20 other brands are looking to capture the growing "smart shoe" market by looking for affordable ways to revolutionize the shoe. One way to expand the capability of shoes that will also provide useful information to their physically active consumer base is to incorporate force sensors. For example, these force sensors will tell a runner if they are a forefoot or rearfoot striker – information that can help transform them into a more efficient runner. Affordable force sensing shoes can also help marathon runners determine if they begin switching from forefoot to mid or rearfoot ever during their run. For athletes that are active for such long periods and long distances like marathon runners, having sensor that move with them and don't impede their training are very useful in optimizing their performance. And though there has been significant research done in

plantar anatomy and physiology as they relate to athletic performance, scientists have yet to reach a consensus on the effects of foot type and architecture in foot-related athletic injuries [25]. For questions such as this, being able to detect plantar pressure on different terrains is helpful.

Current sensing configurations used for plantar sensing studies are one of three types: pressure distribution platforms, imaging technologies, or in-shoe systems [1]. The Gait Checker (GHW-1100), Pedar-X® system, and the Tekscan F-Scan™ system are some real-world examples of plantar sensing techniques. Though these sensors have good accuracy and sensitivity, they are either for lab settings only or are incredibly expensive. As a result, there is a limited range of studies scientists can run within the constraints of available sensors.

Having a stationary platform sensor that can only be used in lab settings does not capture the full range of information involved in highly dynamic activities. Athletes are required to restrict their movements to step over force plates or move within motion capture systems. This can inadvertently affect the test subject and restrict scientists from capturing the movement data they wish to capture. Platform sensor architectures are also used for barefoot measurements which means it can only be used in studies that inherently exclude the effects of footwear in their considerations. Though there are mobile options on the market integrated into footwear, they are expensive. Some sensors reach up to the tens of thousands of dollars for just the sensor (without the accessories). The high cost for this type of equipment limits the number of people who can purchase it, which ultimately restricts the type of experiments being run. There are currently no high-accuracy, affordable sensors that are easily integrated into mobile activities on the market today. However, if these sensors were a reality, then everyday athletes could wear these sensors and capture training data in real-time to optimize their workouts.

Currently, research is being done in the Biomimetics Robotics Lab at MIT into force sensing shoes. The current version of the shoes uses multiple cylindrical force sensors located at critical pressure points on the foot. These sensors utilize the Stress Field (SF) method which infers the applied load based on the stress distribution inside a elastic material like

rubber. This sensor design is robust to high impacts from repeated foot strikes and inertial noise from repeated leg swings. There are two versions of the current sensor design. They differ in diameter for the ball (45mm) and heel (65mm) of the foot and are both are approximately 20mm in thickness. Though the current design is relatively comfortable for footwear applications, a thinner profile is desirable.

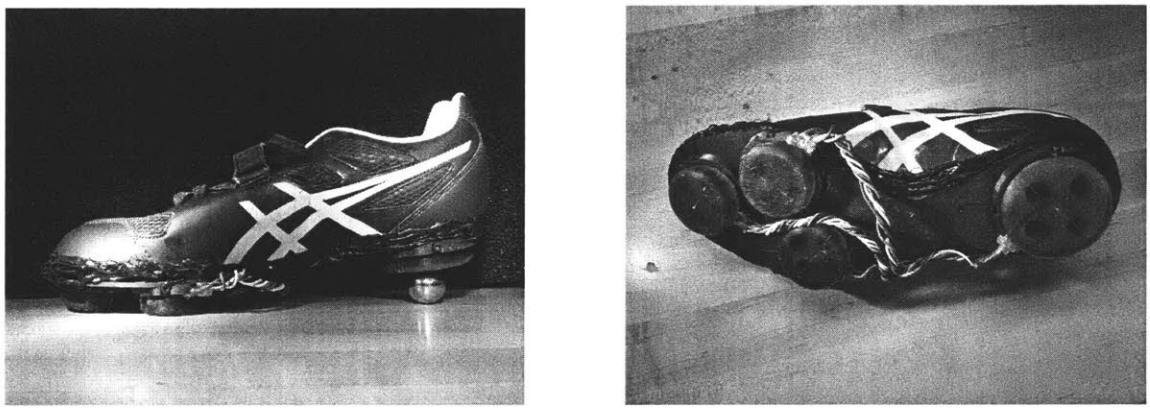

Figure 1.3: Force Sensing Smart Shoes Developed by Dr. Meng Yee (Michael) Chuah in the Biomimetics Robotics Lab at MIT. Left: A side view of the second iteration of the smart shoes. **Right**: A view of the soles of the smart shoes. Three smaller cylindrical sensors are centered around pressure points in the fore foot while one larger cylindrical sensor measures forces in the heel. Photos courtesy of Biomimetics Robotics Lab.

1.3 Desirable Sensor Features for Medical Purposes

One method of evaluating foot health is by analyzing plantar pressure characteristics. Such information can be used to evaluate footwear or diagnose gait abnormalities. In fact, one of the earliest applications for plantar pressure measurements was to analyze footwear. In 1997, Lavery et. al. used these measurements to compare therapeutic and athletic shoes with and without their viscoelastic insoles [1]. In 2000, Lobmann et. al. observed the effects of preventative footwear on foot pressure in diabetic patients [18]. In the area of disease diagnosis, studies such as that done by Nawata et. al. used plantar pressure data to examine athletes with ankle joint instability [20]. Queen et. al. determined that patients with flat feet were more likely to sustain medial and lateral foot injuries such as metatarsal stress fractures

from digital scanning and in-shoe systems [25]. And Zou et. al. were able to determine the relationship between subsurface stresses and skin breakdown in patients with diabetic mellitus and peripheral neuropathy with plantar pressure data [37]. For studies such as these, it is crucial to develop accurate sensing technologies to capture foot pressure data. Accurate sensing equipment has a tremendous effect on footwear products on the market as well as medical treatments for foot-related ailments.

Looking more closely into the area of foot-related medicine, it is apparent that many research studies focus on foot ulceration in patients with diabetes. Diabetes mellitus causes mechanical dysfunction and irregular pressure distributions in feet by progressively weakening foot muscles and sensations (also known as peripheral neuropathy). Foot ulceration in patients with diabetes is one of the leading causes of disability and causes the longest hospitalization periods out of all diabetic complications [18]. In the United States, diabetes mellitus accounts for over $1 billion in medical expenses per year and is expected to affect over 366 million people by 2030 [1]. The study done by Lobmann et. al. determined that early insole support was helpful in reducing plantar pressure and recommended that patients readjust their specific insole every 6 months [18]. Another study done by Boulton et. al., which found that all studied patients with previous foot ulcerations had abnormally high foot pressures at the ulcer sites, determined that predictive measures were helpful in treating areas prone to foot ulceration [4]. If diabetic patients are able to constantly monitor their plantar pressure by having plantar pressure measurement capabilities incorporated into their footwear, then the rate of ulceration can be decreased even further.

1.4 Desirable Sensor Features for Robotics

In robotics, the field of tactile sensing has primarily focused on dextrous manipulation for robot hands. Robots are able to accomplish complex in-hand manipulation tasks in partial thanks to tactile sensing advancements. Tactile sensing is important in manufacturing where tasks involve heavy and/or repetitive tasks that are unsafe for human technicians. As shown

Table 1.1
Design Criteria for Dextrous Manipulation. Table courtesy of Kappassov et. al. [15].

Criteria	Pros	Cons	Applications
High spatial resolution	A smaller objects can be recognized and features with a higher precision can be extracted.	A smaller sensitivity and a longer processing time.	Contact pattern recognition, fine manipulation.
High sensitivity	Detection of a rather small change of a contact force.	Dynamic range of the sensor shrinks, spatial resolutions decreases.	Light touch detection and fragile object manipulation.
High frequency response	A rather fast response to the changes in the level of the contact force.	Spatial resolution and dynamic range.	Detection of a slip and texture recognition.
Low hysteresis	High frequency response	Decrease of the sensor's surface friction and dynamic range.	Detection of a slip and texture recognition.
Low number of wire connections	The workspace of robot hands does not change.	Decrease of the frequency response (in case of using serial data communication).	Dextrous manipulation
High surface friction	Ensuring stable grasp without applying high forces.	Impede tactile exploration procedure. Reduces the frequency response of the sensor (in case of using soft paddings).	Grasping

in Table 1.1, the specific requirements of tactile sensing for robotic hands are high spatial resolution, high sensitivity, high frequency response, low hysteresis, few wired connections, and high surface friction. These sensors are specifically designed to detect small magnitude and changes in force, which is reflective of hand-inspired sensing. The sensing requirements for plantar applications are slightly different, and this is apparent when looking at sensing in human hands and feet. In humans, though the number of mechanoreceptors in the hand and feet are proportionally similar, the activation threshold of mechanoreceptors in the hand are much lower than those in the foot [16]. In layman's terms, the hand is much more sensitive to light touch than the foot. As a result, the sensing requirements for plantar tactile sensors are largely similar to those of hand-inspired sensors. The main differences are that plantar sensors need to withstand much higher loads at the cost of high spatial resolution and require high sensitivity for fast balance correction.

Plantar tactile sensing plays an important role in humanoid, legged robots, specifically as a source of feedback. Many legged robots use force/torque sensors, which are sensors that

are able to measure forces from all directions, to back-calculate the reaction forces. However, these sensors are highly susceptible to inertial noise which create phantom forces that can confuse legged robots. Inertial noise is a result of high acceleration from the swinging legs and are an inherent problem in force/torque sensors. The inertial noise can obfuscate the reaction force data with noise and prevent the robot from detecting contact forces [6]. Figure 1.4 shows that inverse dynamic calculations from force/torque sensor readings produce large amounts of noise that obscure the actual force data.

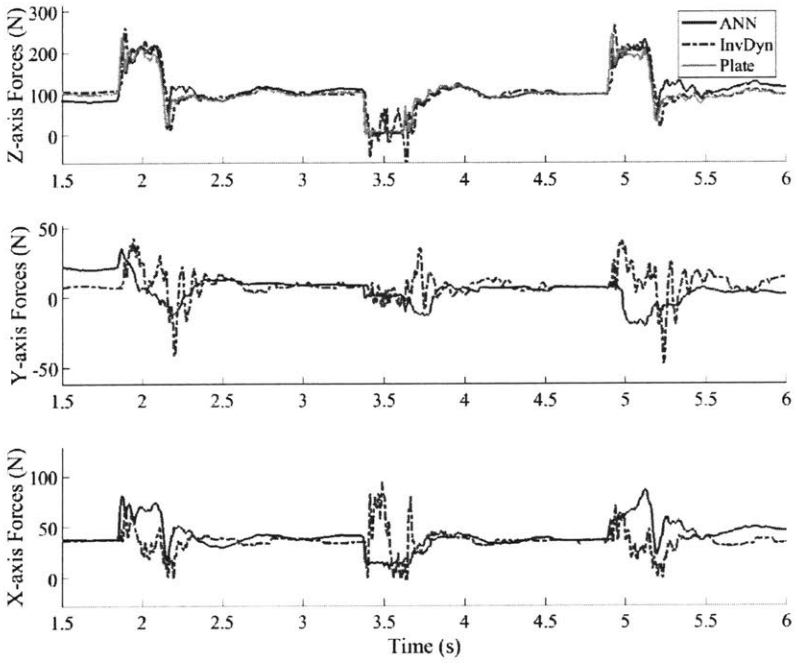

Figure 1.4: Experimental Data of MIT Cheetah 3 during Trotting. The plots show the discrepancy between measured forces from force plate data (yellow), estimated forces from a neural network (blue), and proprioceptive forces from inverse dynamics via a force/torque sensor (red). Image courtesy of MIT Biomimetics Robotics Lab.

The HERMES Humanoid System, which is a tele-operated humanoid robot for search and rescue purposes, is one specific project currently investigating human balancing strategies. The robot functions by sending and receiving force feedback to a human operator. As far as plantar and balance feedback goes, HERMES uses a Balance Feedback Interface to communicate its current state back to the operator. However, the system requires the

operator to continuously stand on a force plate in order to capture the operator's CoP data to send to the robot. The robot also currently uses force/torque sensors to relay its balance data back to the operator, but is in the process of integrating plantar tactile sensing [6].

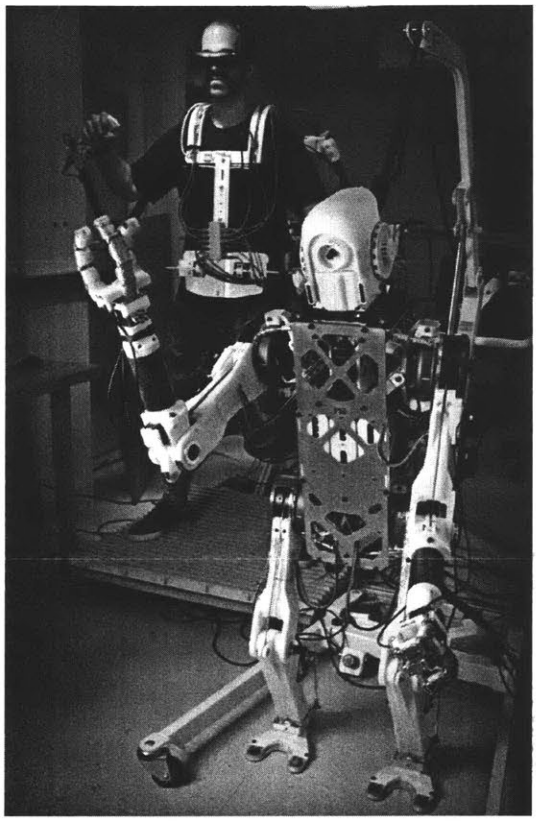

Figure 1.5: The HERMES Humanoid System and operator (background). The use of plantar sensing in HERMES will allow the operator to better understand the robot's environment and provide better balance feedback. Photo courtesy of MIT Biomimetics Robotics Lab.

1.5 Sensing Method Backgrounds

There are numerous tactile sensing techniques currently available. These transduction techniques include capacitive, resistive, piezoelectric, inductive, and optical methods. Table 1.2 summarizes these transduction techniques as well as their advantages and disadvantages. This thesis will investigate piezoresistive and hall-effect methods in particular.

Table 1.2
Comparison of Existing Sensing Techniques. Data courtesy of Tiwana et. al. and Yousef et. al. [30, 36].

Sensor Type	Modulated Parameter	Advantages	Disadvantages
Resistive - Strain Gauge	Change in resistance	• Sensing range • Sensitivity • Low cost • Established product	• Calibration • Susceptible to temperature changes • Susceptible to humidity • Design complexity • EMI induced errors • Non-linearity • Hysteresis
Resistive - Conductive Polymer Films	Change in resistance	• Mechanically flexible • Robust and chemically resistant • Large-area low-cost fabrication techniques • Simple structures and fabrication techniques possible	• Not stretchable • Low sensitivity • Conduction in all directions so applications often restricted to pressure sensing/imaging
Piezoresistive Elastomer	Change in resistance	• Stretchable • Simple structures and fabrication techniques possible • Can be tailored for specific measurement ranges • High spatial resolution • Structured sensors	• Lower repeatability • Hysteresis • Higher power consumption • Restricted to pressure sensing/imaging • Low sensing range
Capacitive	Change in capacitance	• Excellent sensitivity • Good spatial resolution • Large dynamic range • Temperature independent • 3D force sensing possible	• Stray capacitance • Noise susceptible • Complexity of measurement electronics
Piezoelectric	Strain (stress) polarization	• High frequency response • High sensitivity • High dynamic range • Mechanically flexible	• Poor spatial resolution • Dynamic sensing only • Not stretchable • Sensor output drift
Inductive	Change in magnetic coupling	• Linear output • Uni-directional measurement • High dynamic range	• Low spatial resolution • Bulky • Poor reliability • More suitable for force/torque measurement
Optical	Light intensity or spectrum change	• Good sensing range • Good reliability • High repeatability • High spatial resolution • Immunity from EMI • No cross-talk	• Bulky in size • Non-conformable

1.5.1 Piezoresistive Sensing

Piezoresistive sensors are pressure-based elements that detect changes in resistance via different magnitudes of force. Due to the wide range of materials available for sensor development, these sensors can be fine tuned to specific sensing ranges or sensing properties. In other words, the choice of material can affect the range of force measurement, sensitivity, mechanical properties, and other characteristics of the sensor depending on the desired application [23]. And though typical piezoresistive sensors are based upon more rigid semiconductor materials, this thesis will investigate piezoresistive elastomers in detail.

The sensor element is usually some form of conductive elastomer between two electrodes. The conductive elastomer is created by mixing together some conductive particulate such as carbon black with some type of thermoset elastomer. The elastomer insulates each of the particulates such that they do not conduct any electrical signals to each other. As the elastomer is compressed, the number of conductive particulates embedded in the elastomeric matrix get closer together. After the applied force passes a certain percolation threshold, the particulates from a conductive pathway between the electrodes. With increasing force, the particulates are compressed even further and the number of pathways increase. So, increasing force results in decreasing resistance. The sensor architecture is relatively simple to manufacture and lends itself to array configurations because there is minimal probability of sensor cross talk or electromagnetic interference. However, because of their elastomeric qualities, these sensors are also susceptible to hysteresis. Another peculiar point to this type of sensing solution is that it requires fine tuning of the ratio between conductive particulate to elastomer. It also functions under the assumption that the particulate is homogeneously distributed within the elastomer. As a result of some of these unknown variables, it is difficult to model and predict the behavior of these types of sensors. Some results also report certain problems regarding sensor consistency, such as increasing resistance with increasing force as a result of inhomogeneity of the conductive elastomer matrix. In other words, at some point as the sensor is compressed, the force breaks more conductive pathways than it creates. This means the sensor can only function within a finite strain range [29, 33]. Despite these difficulties, sensors created by Canavese et. al. [5], Engel et. al. [9], Guo et. al [11], Hidalgo-

Lopez et. al. [13], Papakostas et. al. [21], and Woo [33] have shown promising results for different piezoresistive elastomeric sensor architectures.

1.5.2 Hall-Effect Sensing

Hall-effect sensors function on the principle of their namesake phenomenon. They are unlike inductive sensors in that they can also detect static magnetic fields. Both sensors output a certain voltage given a certain magnetic field, but inductive sensors only respond to changing magnetic fields. Hall-effect sensors are not a common sensing modality among current tactile sensing technologies. This can be due to a number of factors. For one, Hall-effect sensors depend upon the presence of some magnetic field. This means that tactile sensor designs must include a magnet embedded in a rubber matrix. The sensor would then detect changes in the magnetic field as the rubber deformed and shifted the magnet's placement relative to the sensor(s). One thing that makes this type of sensor architecture difficult to implement in real-world situations is the risk of interfering magnetic fields. In order to ensure that only the embedded magnet is contributing to the measured magnetic field, the embedded Hall-effect sensor and magnet should be isolated from any stray magnetic field interference. This can be accomplished one of two ways: by physically distancing the sensor from any magnetic elements other than the embedded magnet or by integrating some sort of magnetic shielding material.

Another aspect that makes Hall-effect based tactile sensors difficult to implement is the inherent non-linearity of elastomeric materials. Mapping Hall-effect sensor readings to particular magnet placements is the general method behind Hall-effect tactile sensors. This requires knowledge of how certain force applications relate to the resulting magnet position. The non-linear behavior of elastomers, especially thin elastomers in the case of footwear applications, makes material modeling much more difficult.

Hall-effect based tactile sensing is a relatively recent sensing modality. Despite this and other challenges, Hall-effect based tactile sensors in the field of robotics have produced some

promising results. The Hall-effect integrated plantar sensor with elastomeric padding from the Biomimetics Robotics Lab at MIT physically isolates each magnet to a single sensor and uses deflection of the elastomeric padding to create changes in the magnetic field [7]. The MagOne sensor, which uses one magnet and a 3D Hall-effect module embedded in a elastomer body, is used to investigate design optimization strategies for Hall-effect tactile sensors [3]. Finally, the three-toe biped foot uses elastomeric footpads attached to cantilevered flexures embedded with magnets; the deflection of these flexures correspond to the deflection measured by the Hall-effect sensors [10].

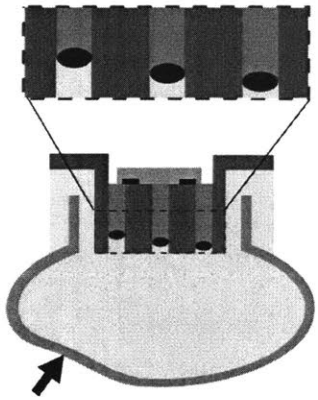

Figure 1.6: Hall Effect Integrated Plantar Sensor with Elastomeric Padding. This sensor from the Biomimetics Robotics Lab uses elastic deformation of the padding in the wells to shift magnets and alter hall effect sensor measurements [7]. Image courtesy of the Biomimetics Robotics Lab.

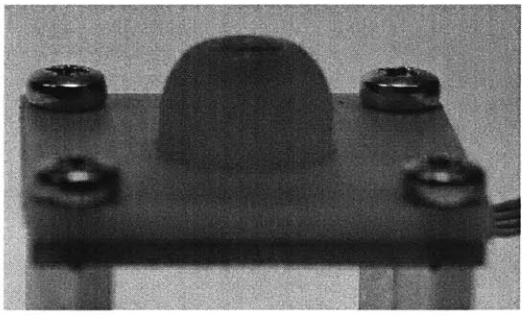

Figure 1.7: MagOne Hall-Effect Based Tactile Sensor. This sensor design project aims to optimize hall-effect tactile sensor designs for general purposes [3]. Photo courtesy of de Boer et. al.

Chapter 2

Piezoresistive Rubber Sensors

2.1 Material and Component Selection

The elastomer materials of interest in this study are Vytaflex 20, Vytaflex 40, Vytaflex 60, and Ecoflex 00-10 from Smooth-On. The conductive particulate materials investigated in this study were milled carbon, carbon fiber, graphite, silver nanoparticle ink, C-200 Carbon resistive ink, VULCAN® XCmax22™ carbon black, and VULCAN® XC72R™carbon black. In addition to different base sensor designs, different copper mesh weave densities for the conductive pads were also considered.

Vytaflex rubbers have high wear resistance and durability, which make them especially well-suited for plantar sensing applications. The numbering for the Vytaflex line, variants of polyurethane rubber, corresponds to the Shore A Hardness. Vytaflex 40 and 60 tended to create piezoresistive sensors with higher force ranges than their softer counterparts. This makes sense as higher ratings for hardness correspond to stiffer materials. Stiffer conductive elastomers are also able to withstand higher force loads before saturation as it requires more force to compress a stiffer sensor the same amount as a more compliant one. They also experience lower amounts of hysteresis.

The intent behind testing Ecoflex 00-10, a type of silicone rubber, was to investigate its high compliancy as a way of increasing sensitivity. This material could undergo larger

deflections than its polyurethane counterparts for the same force application. In other words, this would mean that larger changes in the resistance value would correlate to smaller changes in force. However, softer materials experience larger amounts of hysteresis. Their behavior is more complicated to model and predict. In addition, silicone rubbers have typically low abrasion and tear resistance. So, in order to use silicone rubber for plantar sensing, though not investigated in this design study, it would be wise to encase them in polyurethane or another type of durable thermoset to increase sensor longevity. The second elastomer layer also serves to help stiffen the overall sensor as Ecoflex 00-10 sensors tended to saturate much quicker.

The conductive particulate materials investigated in this study were milled carbon, carbon fiber, graphite, silver nanoparticle ink, C-200 carbon resistive ink, VULCAN® XCmax22™ carbon black, and VULCAN® XC72R™carbon black. These various materials were combined with the rubber at various ratios, with conductive particulates ranging from 10–50 percent of the total mixture's mass. Depending on the material, extra processes were added such as grinding the materials to a finer powder or adding compatible silicone thinner. These processes were necessary to create pourable mixtures for molding. The most promising of the materials investigated were the two variants of carbon black. The resulting sensors produced were chemically stable and produced the most predictable results. They were also the easiest to fabricate as resulting elastomer mixtures were a workable consistency and did not denature after curing.

To test these materials and elastomers without needing to create accommodating sensor bases, various combinations of each elastomer and particulate were created as small samples. Figure 2.1 shows one of these samples as well as the trays that were used to mold the samples. After measuring the appropriate amounts of elastomer and particulate by weight and mixing, each sample was put in a vacuum chamber to remove air bubbles. Then the samples were poured into trays and allowed to cure. These samples were then tested using a multimeter for resistance measurement range and sensitivity to compression. Promising samples were then used to test the various sensor base designs, Multiple sensors were created for each sample mixture and tested for signal behavior and consistency across samples.

Figure 2.1: Typical Piezoresistive Material Test Sample. Different variations of polyurethane and silicone thermosets were combined with several different conductive particulates. Here, Vytaflex 40 was combined with specialty carbon black at 15 percent total mass. The resulting samples were then judged for quality of cure and piezoresistive properties.

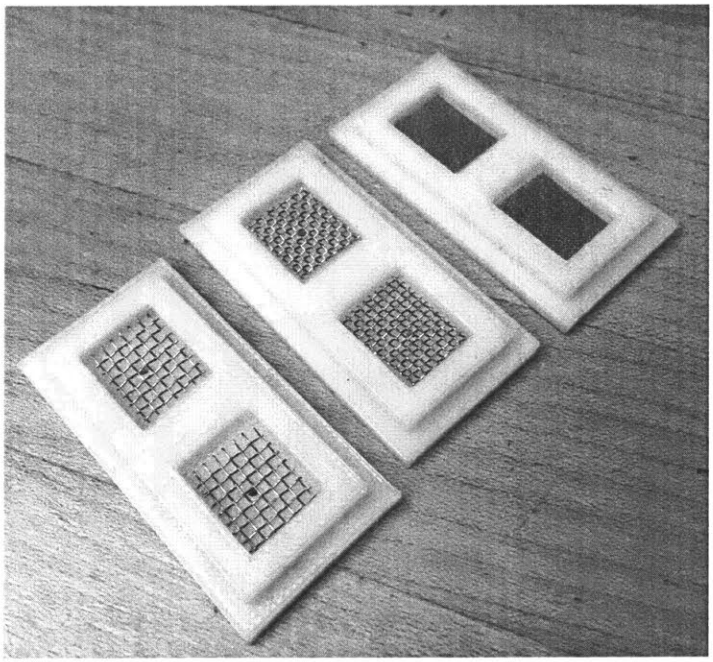

Figure 2.2: Different Copper Mesh Weave Densities in Piezoresistive Sensor Design V1. Tested copper weave densities from left to right: 16x16 per inch, 22x22 per inch, 80x80 per inch.

Increasing the weave density of the copper mesh pads increases total contact area between the conductive elastomer and the mesh. This means the denser pads capture more of the connections made by the compressed particulates. However, increasing weave density also increases the effect of surface tension. This prevented the elastomer from making full contact with the copper mesh pad. Figure 2.2 shows the variety of copper pads that were investigated. Figure 2.3 pictorially explains the surface tension behavior. To compensate for this, during fabrication, the mesh pads were presoaked with the elastomer mixture. This process involved rubbing the copper pads with the mixture to force material into the crevices of the mesh. All tested sensor architectures were made using copper mesh with 80x80 wires per inch. These pads were lined on two orthogonal sides with leaded solder to ensure electrical connection between wires. The resulting pad was then soldered to a wire for easier measurement.

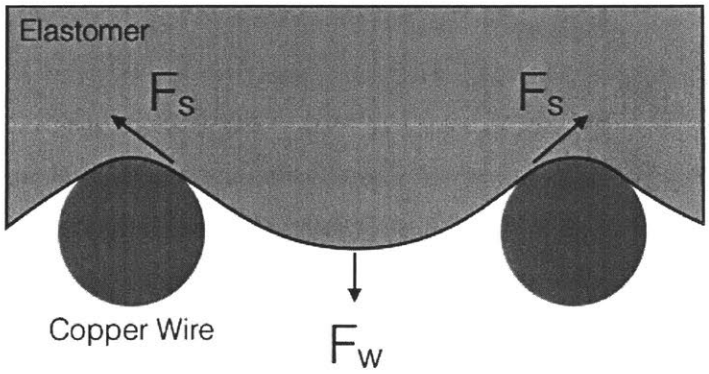

Figure 2.3: Diagram Explaining Relationship Between Copper Weave Density and Surface Tension. As the density increases and the spacing between wires shrinks, then the total force due to weight per open cavity between weaves decreases.

2.2 Fabrication

For shoe-integrated plantar sensors, the sensor needs to not only have good accuracy and sensitivity but also be durable and thin to accommodate to current shoe designs. The two tactile sensing methods investigated both fit within these design constraints. The basic fabrication process for each piezoresistive sensor design can be separated into two parts: the sensor base construction and the elastomer mixture preparation. The sensor base as-

sembly process involved preparation for all the non-elastomeric components including the 3D printed base, copper mesh pads, and wiring. The elastomer mixture process involved preparation of the elastomer components, the conductive particulate, and elastomer thinner (if necessary).

This thesis will investigate five different proposed sensor base designs and analyze their advantages and disadvantages. The production process started with the sensor base design. Most of the sensor base designs investigated were two-part designs. Two-part designs involved a sensor body used to house the copper pads and a fence piece used to contain the rubber. The fence piece allowed for extra rubber material to be poured over the top of the sensor body. The fence piece could be removed once the entire sensor was fabricated. Once the sensor base design was printed on the Stratasys uPrint, the copper pads were cut to fit and assembled. Each of those designs used the same configuration of copper mesh pad and wiring. The copper mesh pads were 80x80 wires per inch. The pads were cut to fit within the dimensions of its designated sensor. The pads were soldered on two orthogonal sides to ensure electrical connection between the copper mesh wires. The pads were then soldered to a insulated, solid core wire for easier multimeter measurement.

The elastomer mixture preparation for sensor fabrication involved a similar process to the elastomer sample. The two parts of the appropriate thermoset were measured out by weight. One part was mixed together with the appropriate amount of conductive particulate. Once thoroughly mixed, the second part of the elastomer thermoset was poured in and combined until homogeneous. If the resulting mixture was too viscous to be poured, controlled amounts of acetone or thinner were added. The mixture was then placed in a vacuum chamber to remove majority of the air bubbles. Finally the mixture was poured into the sensor molds sprayed with mold release and allowed to cure. For two part sensor bases, once the rubber cured, the fencing piece used to contain the rubber was removed.

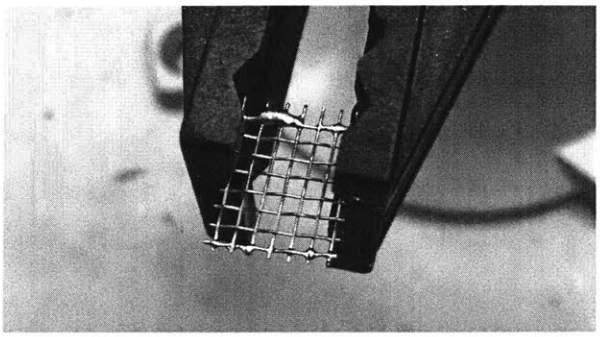

Figure 2.4: 16x16 Copper Mesh Partially Coated with Solder. Each of the copper mesh pads were lined with solder to ensure electrical contact between each weave. The final copper mesh pad would have solder coatings only along two orthogonal sides to ensure electrical connection between all the wires. The pad was then soldered to a wire for easier measurement using a multimeter.

2.2.1 Sensor Design V1

The first version of the piezoresistive elastomeric sensor design was based previous work done by former Biomimetics Robotics Lab member John Mayo. The prior design included two wells for the copper mesh pads and a median barrier to ensure conductive pathways only formed in the rubber matrix above the pads and not directly between them. It also functioned to keep the pads from shifting while the rubber matrix was poured. The prior version was also much smaller, with the long edge of the sensor being approximately half of an inch. The first version (V1) of the sensors being investigated was approximately two inches on the long edge. Though it was much larger than the desired size for its application, it mainly served as a proof of concept and starting point for future iterations. Figure 2.5 shows the CAD model of the original piezoresistive sensor design.

The design came in two pieces. One piece served as the base for the sensor as well as the containment unit for the copper pads. The copper pads were surrounded by a raised platform in order to fixture the pads as well as control the conductive pathways formed. The removable fence piece functioned in the same capacity as the high outer walls of the prior design. However, unlike the previous design, because the fence was removable, the rubber was unconstrained and allowed to deform freely. Figure 2.6 shows fully fabricated version of the V1 sensor with and without the rubber containment fence.

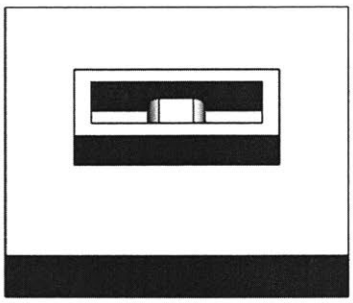

Figure 2.5: CAD Model for Piezoresistive Sensor V1 Inspiration. Like V1, this sensor uses horizontally aligned copper mesh pads placed on the same plane and is encased in elastomer. The two flat areas within the sensor walls are the copper pad locations. The raised protrusion helps control the conduction path of the compressed particles.

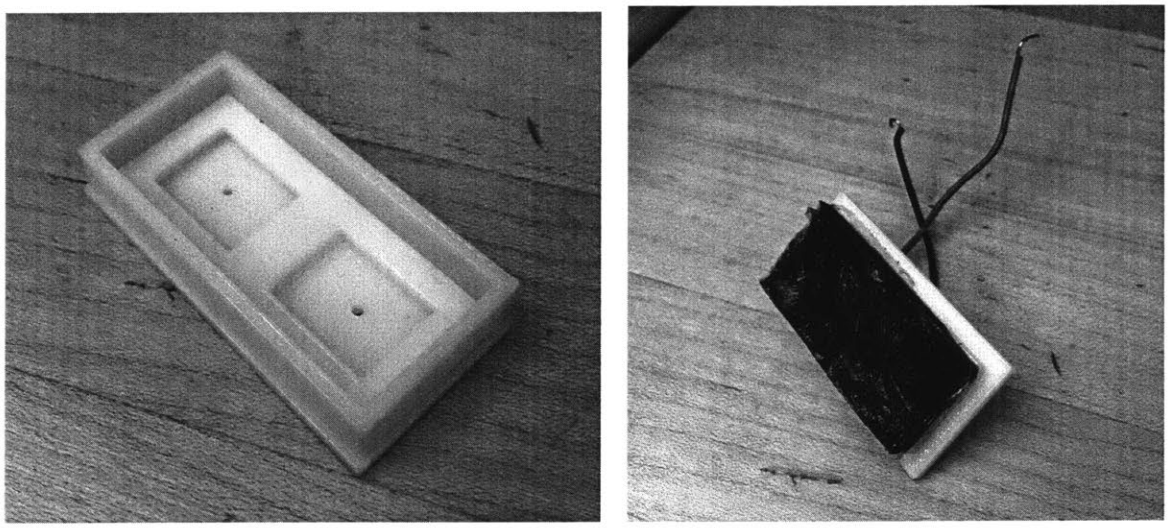

Figure 2.6: 3D Printed Piezoresistive Sensor Base and Fence V1 and Final Sensor. Left: Sensor base and removable elastomer fence with two wells for copper mesh pads. **Right**: Sensor base with carbon fiber and elastomer matrix.

This was an improvement, but the design also elucidated some important considerations. For one, the sensor was used to primarily test Vytaflex 20 mixtures. The material was discovered to experience significant amounts of viscoelastic creep, which was extremely problematic for a highly sensitive, piezoresistive sensor design. In other words, for a sensor that depends on materials properties, in order to quickly detect changes in force, materials that are slow to equilibrate to imposed forces are undesirable. The material's resistance also did not scale linearly with the increasing amounts of applied force. Closer examination of the design also revealed two things. For one, the rubber mixture cured in such a way that allowed the conductive particulates to slowly stratify in the rubber due to their differing densities. This meant that the rubber was likely not as homogeneous as originally intended. It also made clear that its size made it difficult to detect point forces or forces that only acted on half the sensor.

2.2.2 Sensor Design V2

The V2 design maintained the horizontal orientation of the copper mesh pads in V1, but instead stacked them on top of one another. In this orientation, the conduction paths formed parallel to the applied force vector. The new sensor also shrank in physical size. The sensor measures approximately three-quarters of an inch on the long side and is approximately the same in height compared to V1.

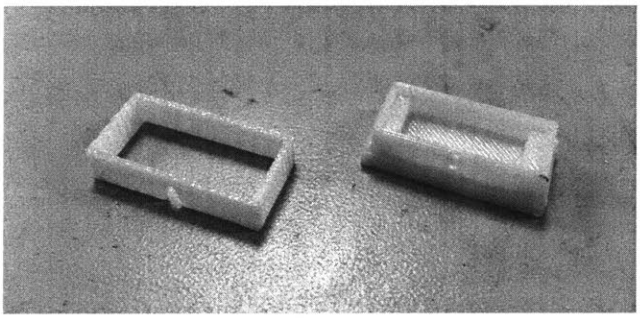

Figure 2.7: 3D Printed Piezoresistive Sensor Base and Fence V2. This version of the sensor base design used horizontally aligned copper mesh pads and stacked them on top of one another parallel to the axis of force application.

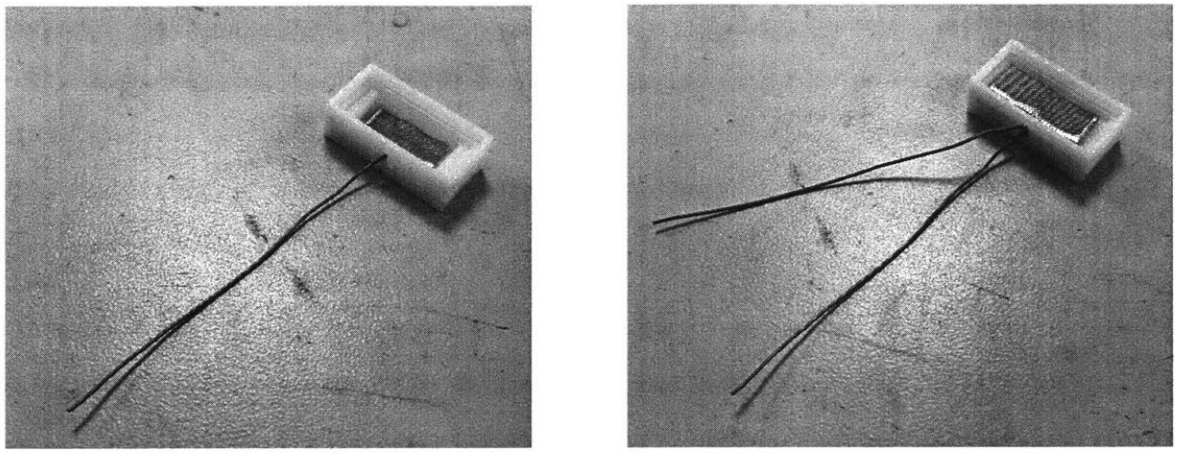

Figure 2.8: Piezoresistive Sensor Base and Fence V2 with Copper Mesh Pads. Left: Sensor base with bottom copper mesh pad. **Right**: Sensor base with bottom and top copper mesh pads. The top copper mesh pad is supported by two 3D printed ledges integrated with the sensor base.

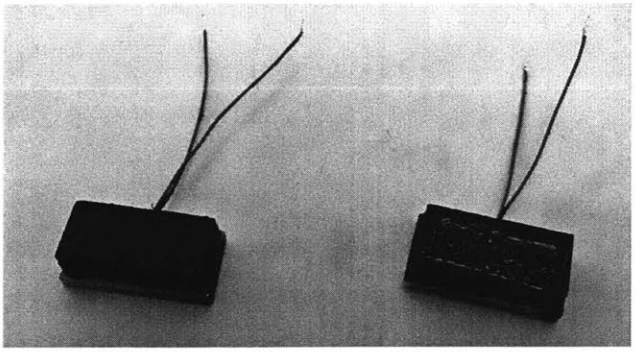

Figure 2.9: Piezoresistive Sensor Base V2 with Carbon Black and Elastomer Matrix. For V2 sensors, the copper pads are horizontally aligned, but stacked on top of each other versus the V1 design where the copper pads were horizontally aligned but on the same plane.

The fabrication process also involved a two-part sensor design. However, the base and fence piece had to accommodate for the reorientation of the solid core wires by including small holes. In V1, the wires protruded from the base of the design which made it difficult to place the sensor on flat surfaces. This was fixed in V2 where the protruding wires were redesigned to come out of the side of the sensor. The sensor base also had two elevated platforms to support the upper copper mesh pad while the lower copper mesh pad sat on the bottom face of the base. Figure 2.7 shows the bare sensor base architecture prior to the

elastomer pour. Figure 2.8 shows the orientation of the copper mesh pads within the sensor base. Figure 2.9 shows the final fabricated sensor.

2.2.3 Sensor Design V3

The V3 design focused on shrinking the overall sensor and placing the copper mesh pads in a different orientation. Like V1 and V2, this version was also a two-part sensor. The sensor dimensions were the same as those of V2. The mesh pads were placed in a horizontal fashion and kept in place by small protrusions designed into the base to press the pads as close to the opposing ends of the sensor as possible. The wire protrusions were designed to come out of the short sided faces of the sensor. The sensor pads were moved in order to investigate the relationship between direction of conduction path formation and direction of force application. The change appears to have minimal effect if not overshadowed by other factors. Figure 2.10 shows the fabricated V3 sensor.

This design primarily tested Vytaflex 40 and 60 carbon black samples. They also produced inconsistent resistivity ranges across identical units. These sensors were also subject to further force response testing.

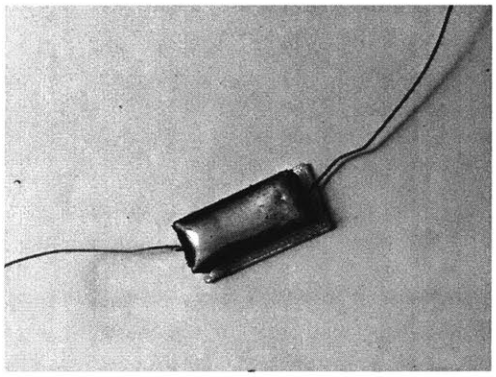

Figure 2.10: Piezoresistive Sensor Base V3 with Carbon Black and Elastomer Matrix. For V3, the copper mesh pads are aligned vertically and placed on opposite ends lengthwise on the sensor.

2.2.4 Sensor Design V4

The V4 design was a smaller version of the V3 sensor. The overall architecture was similar; the main difference was its dimensions. The sensor was approximately half of an inch on one side and about half the height compared to V2 and V3. Like the previous two versions, V4 was also a two-part design. It primarily tested Vytaflex 40 and 60 carbon black samples as well. And similarly to V3, the resulting signals were responsive to changing forces in V4, but were produced inconsistent resistance values in identical sensors. Figure 2.11 shows the fabricated V4 sensor.

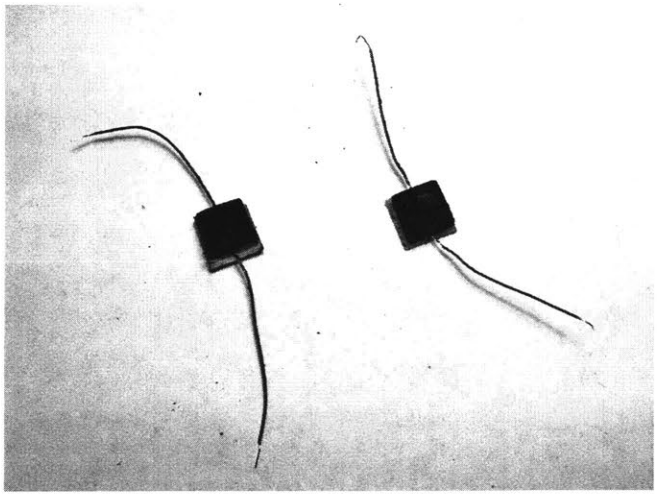

Figure 2.11: Piezoresistive Sensor Base V4 with Carbon Black and Elastomer Matrix. Like V2, V3 sensors have vertically aligned copper mesh pads, but the overall thickness is much smaller.

2.2.5 Sensor Design V5

This sensor design went in a completely different direction than the other designs. This design did not have any 3D printed sensor base integrated into the final sensor. Instead, the design used a 3D printed container sprayed with mold release that would be removed and reused to create more sensors. The container was a one inch tall, thin-walled box design. Much larger copper pads were used. They were placed on opposing faces with the largest area to maximize the number of conduction pathways. Another thing that was unique about

this design was that the elastomer was poured in a direction orthogonal to the direction of force application in the final sensor. This was to accommodate for the likely stratification of conductive particulates in the elastomer as the mixture cured overnight. When the sensor finished curing and was removed from the container, the sensor would be turned on its side and would be ready for use. An example of the final sensor can be seen in Figure 2.12.

This sensor displayed promise but did not undergo the same amount to testing as the previous versions. Further exploration of this sensor design would be the subject of future work.

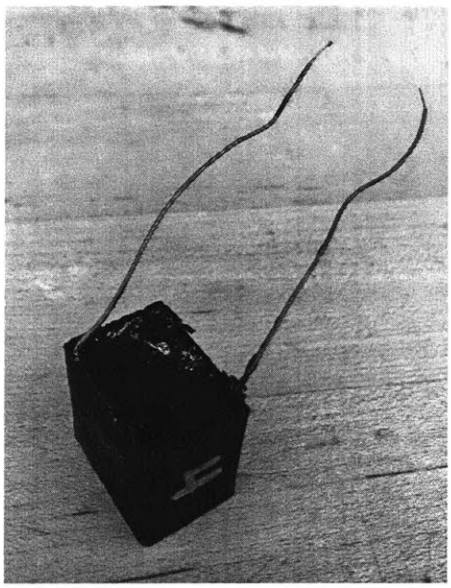

Figure 2.12: Piezoresistive Sensor V5 with Carbon Black and Elastomer Matrix. For V5 of this sensor, the 3D printed sensor base was entirely removed from the design and the copper mesh pads were stacked parallel to the axis of force application.

2.3 Experimental Setup for Data Collection

For preliminary measurements of the elastomer samples, two probes were placed approximately one centimeter apart. The resistance measurement was then recorded and analyzed in comparison to the results from other samples. Promising mixtures were then recreated and molded into sensors. The nominal resistance for each sensor was then recorded. From

there, each sensor was tested for sensitivity in a setup similar to the one shown in Figure 2.13. The sensor was attached to multimeter and the relationship between its resistance and increasing weight were recorded. For sufficiently sensitive sensors, the final test was to place them on a force plate and use a CNC mini mill to apply normal force in a controlled manner. The voltage response was recorded and analyzed for sensitivity and hysteresis.

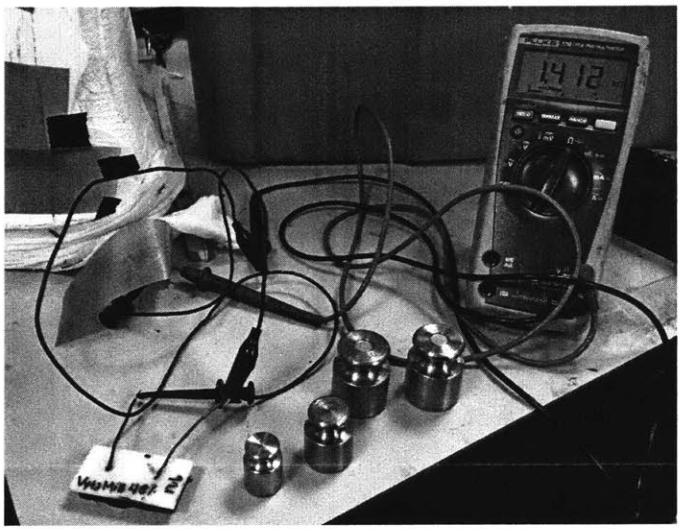

Figure 2.13: Setup for V1 Sensor Preliminary Testing. To qualitatively judge the potential for each sensor, increasing masses were placed on top of the sensor and compared to the resulting resistance value.

Chapter 3

Hall-Effect Integrated Sensors

3.1 Material and Component Selection

3.1.1 Hall-Effect Sensor

The specific Hall-effect sensor used (shown in Figure 3.1) is the Ratio-metric Linear Hall-Effect Sensor (DRV5055 series) from Texas Instruments. These sensors come in four different types varying in sensitivity (and by default, sensing range). Because sensitivity is of key importance in plantar force sensing, this thesis will mainly focus on the A1 sensor.

Figure 3.1: Linear Hall-Effect Sensor from Texas Instruments. These Hall-effect sensors are available in four different varieties with different sensitivities and data ranges. Image courtesy of Texas Instruments.

3.1.2 Elastomer

The elastomer selected for these prototype sensors is Vytaflex 20 from Smooth-On. There are several reasons for the selection of this particular variant of elastomer. One is for its wear resistance. Vytaflex 20 is a type of polyurethane rubber with good impact resistance, making it advantageous for legged locomotion sensing applications. Polyurethane elastomers have high abrasion, cut, and tear resistance. These features make it well suited for applications as a plantar tactile sensor where it endure many types of rough terrain under high impact and shear stress conditions. Polyurethane also has good load bearing capacity which is a preferable characteristic for plantar sensors. It is also a thermoset, which means it a relatively easy material to mold into different shapes. Figure 3.2 shows a tactile sensor from the Biomimetics Robotics Lab that uses internal stress fields in Vytaflex 20 to measure force. This sensor is conceptually similar to the Hall-effect integrated sensor investigated in this thesis.

Though there are many different forms of polyurethane rubber with different material properties, the reason why Vytaflex 20 was selected was because of its balance between compliance and stiffness. Vytaflex 20 has a Shore A hardness of 20, putting it on the softer side of Smooth-On's Vytaflex line. This Hall-effect integrated sensor design uses a magnet embedded in the rubber matrix and detects changes in the magnetic field as the rubber deforms and causes normal and shear deflections. Since this design depends on a thin profile for easy shoe-integration, the dimension of the rubber layer becomes even more crucial. In order to manufacture a sensor with a minimally thick rubber layer, then the selected polyurethane rubber needs to have sufficient compliance. This is to allow the embedded magnet to deflect enough to significantly change the Hall-effect measurements. However, if the material is too compliant, then the minimum force for sensor saturation decreases as it takes less force to compress a more compliant material the same amount as compared to a stiffer material. For a sensor that is expected to undergo relatively large impact forces frequently, having a stiffer material that can withstand those conditions without saturating the sensor is desired. However, If the material is too stiff the magnet may not deflect enough and essentially limit the sensor's data range.

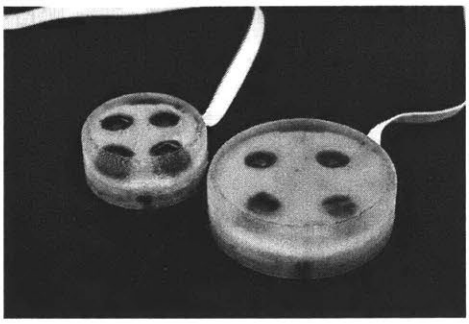

Figure 3.2: Cylindrical Force Sensors with Vytaflex 20. Two size variants of a piezoresistive sensor design are shown here. These two sensors are approximately 45mm and 65mm in diameter and 20mm in overall thickness. The sensors are encased with Vytaflex 20. Image courtesy of Biomimetics Robotics Lab.

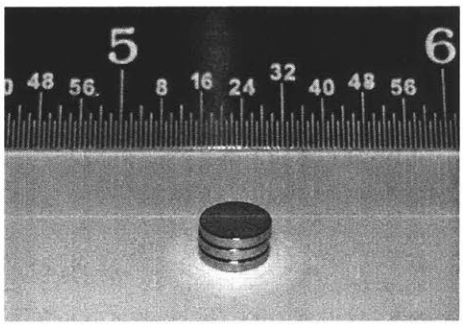

Figure 3.3: Three Neodymium Iron Boron Magnets. These magnets were tested in stacks consisting of one, two, or three magnets.

3.1.3 Magnet

The magnets used for testing were Neodymium Iron Boron (NdFeB) disc magnets that were approximately 6/32" in diameter and 1/32" in height. The magnet was selected for its small size and for its relatively high flux density. The magnets were combined into sets of one, two, or three magnets. Figure 3.3 shows the magnets. The Hall-effect sensors used for the study were tested prior to determine if magnetic shielding material would be necessary. From that test, it was determined that shielding material was not crucial in the first iteration to protect the sensors from magnetic field interference or amplify the existing magnetic field flux. However, in the presence of high magnetic field flux density environments, shielding would be necessary. This is the subject of future work.

3.1.4 Sensor Array Design

Two different sensor array designs were tested. The sensor arrays consisted of four Hall-effect sensors soldered in a square plan onto a custom PCB. One design spaced the Hall-effect sensors 10mm apart from each other while the other spaced them 15mm apart. Both boards also have six external wire connections for data acquisition. Figure 3.4 shows the two different arrays.

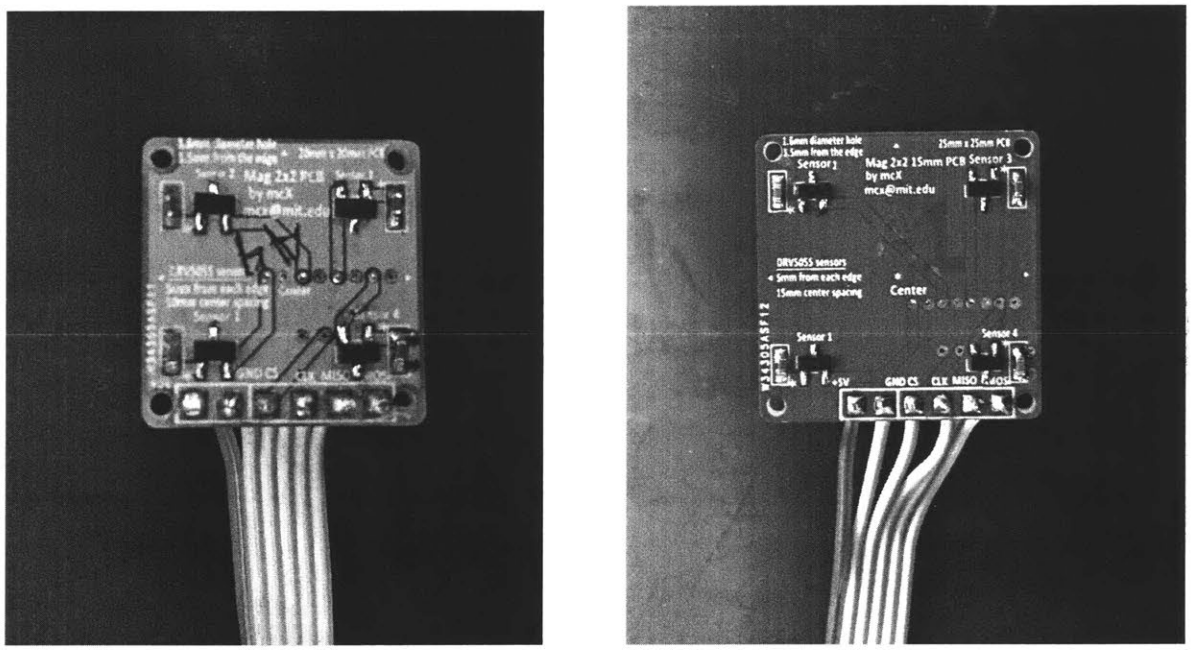

Figure 3.4: Hall-Effect Integrated Tactile Sensor PCB Layouts. Left: 10mm spacing PCB layout. **Right**: 15mm spacing PCB layout.

The four Hall-effect sensors were used measure the magnetic field changes of a single magnetic body via the concept of triangulation. To determine the position of an object in three dimensional space, a minimum of four sensors are needed. Each of the sensors produces a single value that relates to the radial position of the magnet from the sensor. By determining magnet position and relating it to the four sensor readings, the sensor is able to back-calculate the required normal and shear forces to deform the rubber. Figure 3.5 further explains the triangulation concept.

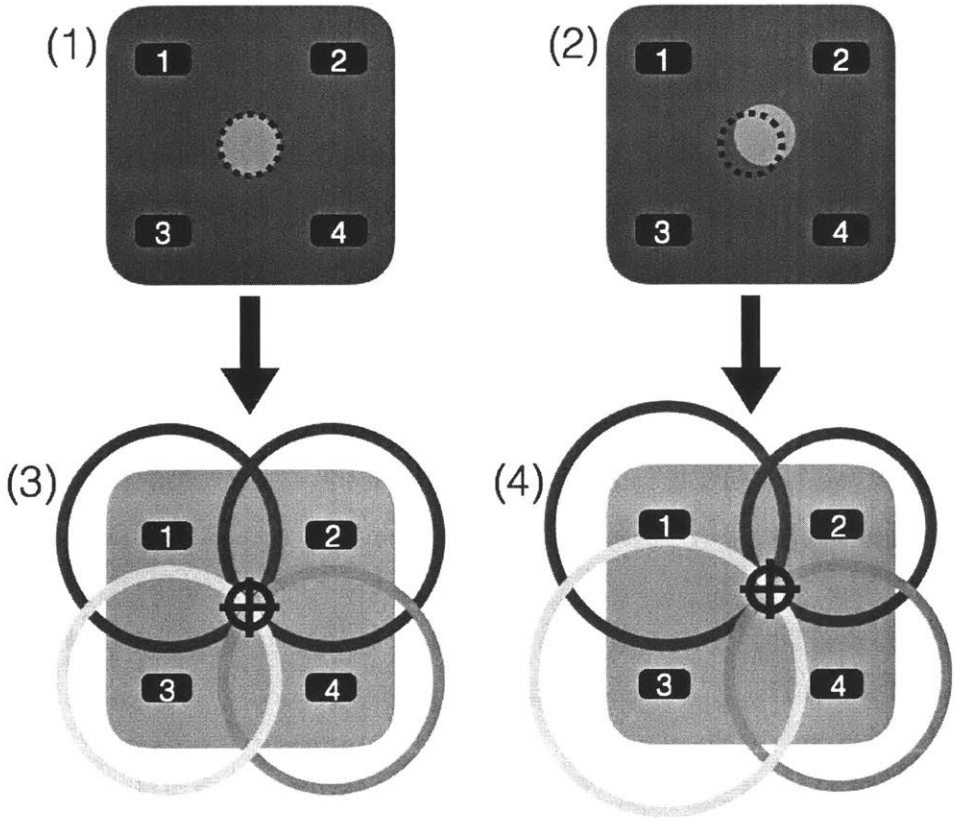

Figure 3.5: Pictorial Representation of Triangulation as used on the Hall-Effect Integrated Sensors. (1): Nominal magnet position. Sensors 1-4 are labelled according to their position in each diagram. The dotted black line represents the magnet's centered position. **(2):** Magnet position after deflection. **(3):** Sensor readings based on magnet position in (1). The colored rings represent the readings for the sensor at the center. **(4):** Sensor readings based on magnet position in (2).

3.1.5 Sensor Fabrication

The first iteration of this sensor design involves encasing the sensor PCB and magnet in Vytaflex 20. CAD models of the proposed sensor design for both the 10mm and 15mm PCBs are shown in Figure 3.6. The following fabrication steps are performed on the 10mm Hall-effect integrated sensor design. The mold is a simple container and PCB back-piece. The container is to house the magnet and extra elastomer material. The Hall-effect sensors on the PCB lie face down into the container of elastomer. The PCB back-piece shields the back of the PCB from the rubber and serves as a flat surface for anchoring onto other surfaces.

Figure 3.7 shows the 3D printed mold and back-piece.

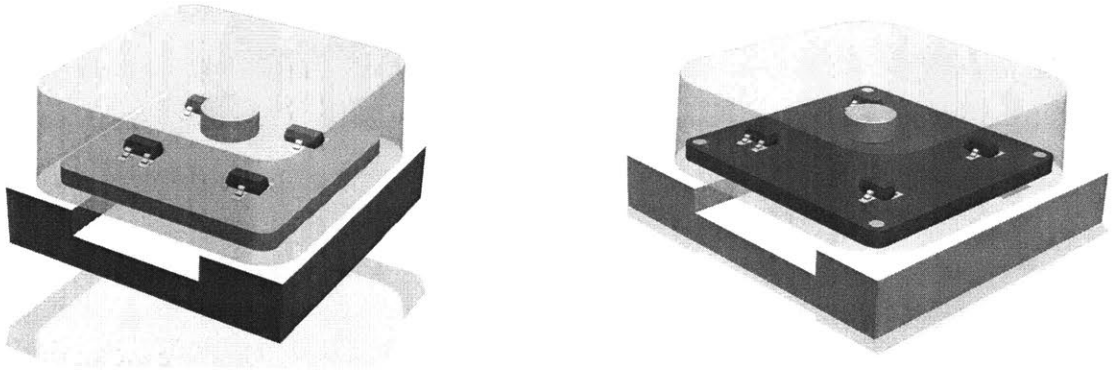

Figure 3.6: Hall-Effect Integrated Tactile Sensor CAD Designs. Left: Proposed design with 10mm spacing between Hall-effect sensors on PCB. **Right**: Proposed design with 15mm spacing between Hall-effect sensors on PCB.

To fabricate this sensor, a small amount of rubber is prepared. The rubber is then placed in a vacuum chamber to remove bubbles. Enough rubber to coat the bottom surface of the container is poured and allowed to partially cure. The magnet is then placed in the viscous mixture. This is to fixture the magnet in a particular position such that when the remainder of the mixture is poured into the container, the magnet will not shift. This step of the fabrication process is shown in Figure 3.8.

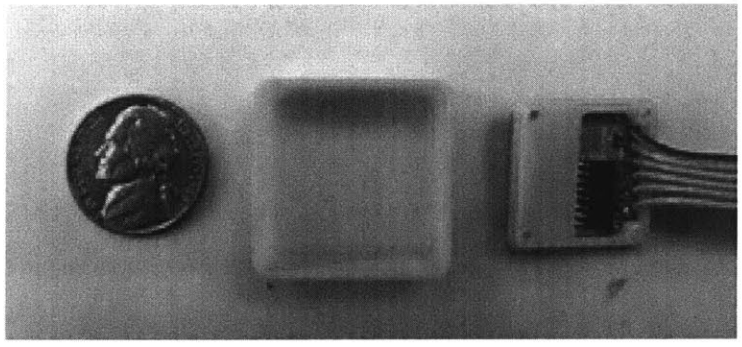

Figure 3.7: 10mm Hall-Effect Integrated Sensor Mold Design The container (center) is to mold the Vytaflex 20. The sensor PCB and PCB back-piece (right) is placed on top of the rubber after it is poured into the container and partially cured. Nickel (left) for comparison. This mold configuration is specifically designed for the 10mm-spaced Hall-effect sensor PCB.

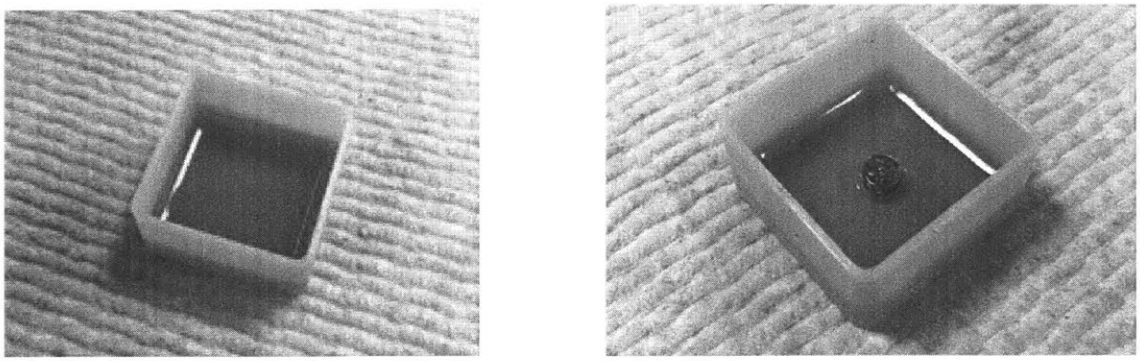

Figure 3.8: Hall-Effect Integrated Sensor Magnet Placement. Left: A small amount of rubber is poured into the mold container and allowed to partially cure. **Right**: The magnet is placed into the rubber. The partially cured rubber fixtures the magnet and prevents it from shifting when the remainder of the rubber is poured into the container.

Once the magnet is placed, additional Vytaflex 20 is prepared and poured into the container. This additional elastomer is then cured such that the mixture is solid enough to minimize shifting but liquid enough to form around the sensor PCB and back-piece. At that point, the PCB and back-piece are placed into the elastomer mixture and fully cured. Figure 3.9 shows the fully assembled mold container, PCB, and back-piece in the process of curing. Figure 3.10 shows the fully cured sensor after removal from the mold container. The final sensor is approximately 15mm in thickness, which is thinner than other previously known cost-effective plantar sensor designs.

Figure 3.9: Hall-Effect Sensor PCB Elastomer Mold. The sensor PCB and back-piece are placed in the Vytaflex 20 matrix and allowed to fully cure.

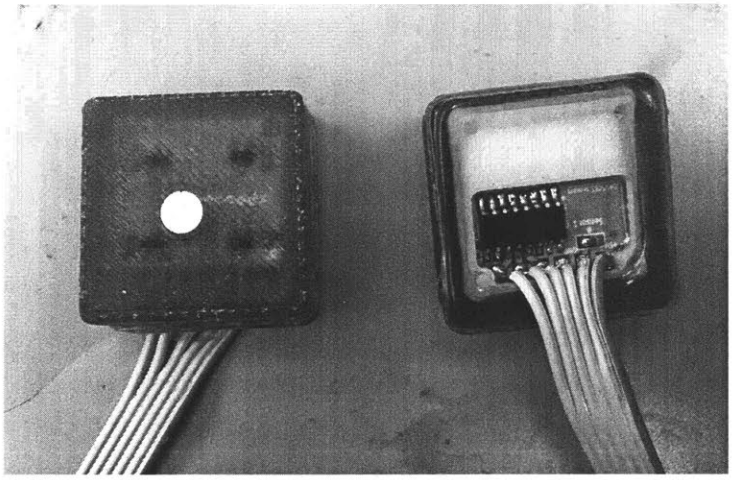

Figure 3.10: Hall-Effect Integrated Sensor This is the first iteration of the Hall-effect integrated sensor design.

3.2 Experimental Setup for Data Collection

3.2.1 Setup

For determining the appropriate magnet for and magnet position relative to the PCB, a CNC miniature mill was used. Before the sensor was molded within a Vytaflex 20 matrix, the bare PCB was fixtured to the CNC mill table while the magnet was fixtured onto the mill spindle. The PCB was fixtured onto the table using a custom delrin block. The block was adhered to the mill table via VHB adhesive. The delrin block was fabricated with a cavity to accommodate for the microchip as well as the protruding wires on the back of the PCB. The PCB was then fitted to the block using plastic dowel pins. The PCB had specifically sized holes designed in to fit the dowel pins. The delrin block had precision-spaced holes drilled in to accommodate for both the 10mm and 15mm PCBs. The dowel pins positioned each of the boards on the block. The block also had a designed protrusion to datum the magnet fixture on the mill spindle to the delrin block. This allowed precision repositioning of the magnet to the center of the PCB after sample switching. Figure 3.11 shows the magnet selection setup.

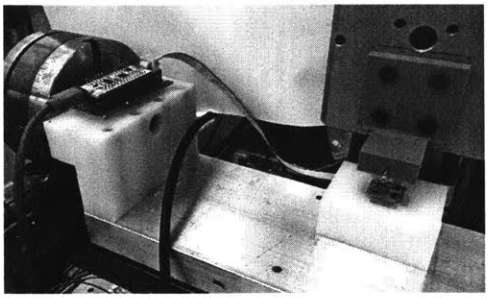

Figure 3.11: Data Collection using the CNC Mill. The Hall-effect sensor PCB was mounted to a custom fixture on the mill table. The magnet stack was fixtured between two acrylic sheets and manipulated using the CNC spindle. A preprogrammed G-Code trajectory was then initiated while data was collected using NI LabVIEW.

The sensor is then hooked up to a data acquisition unit connected to NI LabVIEW. A preprogrammed G-Code path was assigned to the CNC mill. As the mill ran through the code, the data acquisition unit would capture the readings from each of the sensors and plot them versus time. The data output was in bytes with values ranging from 0 to 4096. The nominal value of each Hall-effect sensor (i.e. sensor value in the absence of detectable magnetic field) was 2048. Any value above this nominal value corresponds to a positive value for the magnetic flux. In other words, for magnetic flux that travels from the bottom of the sensor to the top (positive gradient) is considered positive. Any value below this nominal value corresponds to a negative value for the magnetic flux (i.e. negative gradient). This concept is further explained in Figure 3.12.

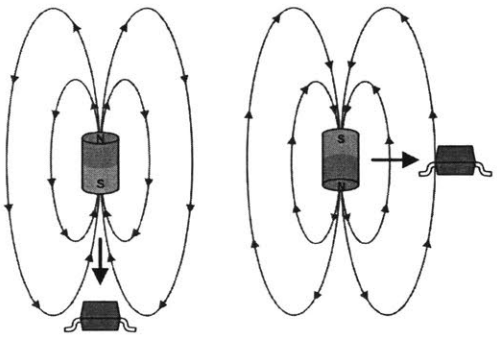

Figure 3.12: Hall-Effect Sensor and Magnetic Field Positioning Diagram. Depending on the location of the magnet in relation to the sensor, the direction of the flux lines changes. This affects whether the raw sensor data detects a positive or negative field. Image courtesy of Texas Instruments.

3.2.2 Magnet Testing

Prior to molding, the magnets were sandwiched inside of an acrylic fixture and tested with the Hall-effect sensor PCBs. Each PCB was tested against one, two, or three magnet stacks to determine which type of magnet setup was most appropriate for this design. Each magnet stack was moved according to a preprogrammed trajectory as can be seen in Figure 3.13. After one run of the circular trajectory, the CNC mill spindle then shifts down in the negative Z direction by approximately 0.1mm before beginning the circular path again. The cycle continues from a Z-axis range of 1.5mm to 0mm above the sensor PCB. The taller magnet stacks produced magnetic field lines with sharper directionality changes while the shorter stacks produced lines with shallower changes. This affected the placement of the magnet measured from the top of the sensor PCB. And though the polarity of the magnet affects whether the sensor produces positive or negative results, because the sensor behaves linearly with the changing magnetic field, the polarity of the magnet was neglected during testing. This means that analysis of the resulting sensor outputs only examined the data ranges between plots. Figure 3.14 directly shows this linear behavior for the DRV5055 series Hall-effect sensors.

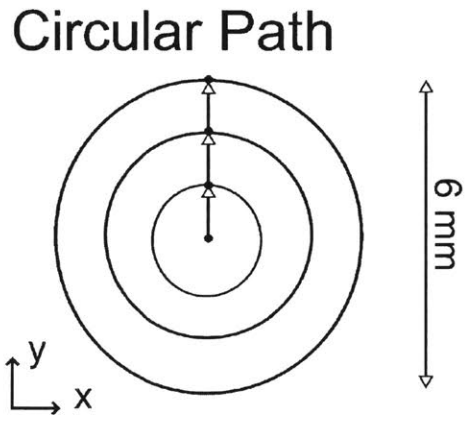

Figure 3.13: Testing Paths for Magnet Selection. The circular path above was used to gather data about the Hall-effect sensor behavior under a changing magnetic field for each magnet stack.

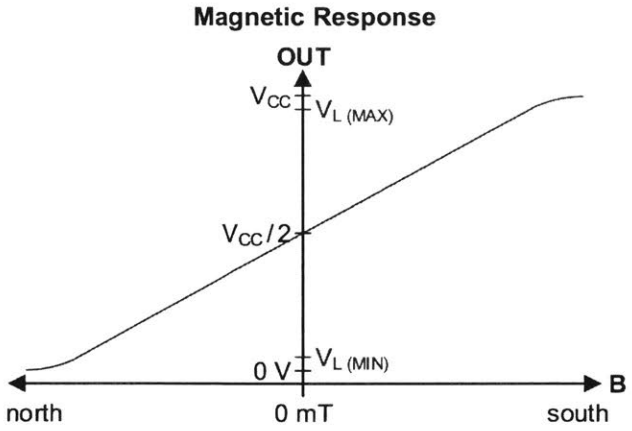

Figure 3.14: DRV5055 Hall-Effect Sensor Magnetic Response. This diagram displays how the sensor's voltage output corresponds with the magnetic flux value. As the magnetic field flux tends toward a maximum or minimum value, the sensor's output voltage tends to saturate. In between these flux values, the sensor behaves linearly, even across the boundary distinguishing positive and negative flux values.

Chapter 4

Results and Discussion

4.0.1 Piezoresistive Sensors

The sensor signals for all the proposed designs were responsive to changes in force, but were clearly susceptible to hysteresis as can be seen in the delayed voltage responses to lower magnitude forces in Figure 4.1. The plot shows the voltage response for a Vytaflex 60/carbon black V3 sensor undergoing a preprogrammed force application operation. The program involved three repeated cycles of three small force bursts followed by three larger force bursts in rapid succession. It is necessary to clarify that larger applications of force translate to lower resistances. Via Ohm's Law, this also means that voltages will also decrease with higher magnitude forces. The profile shows that even the sensors using the stiffest materials were highly susceptible to hysteresis. This can be seen in the three force bursts in every cycle. The voltage in each cycle never returned to the nominal voltage value because hysteresis prevented complete severance of the conduction pathways. Also after the first set of three larger force bursts, one can see a rise in voltage after the third trough. This profile actually represented three smaller force bursts of the subsequent cycle, which was not detected due to hysteresis.

There were two additional preprogrammed operations performed on the same sensor. These additional programs added pauses during and in between force applications in order to examine the hysteresis behavior in more detail. In the single pause program, the force

application was maintained on the sensor for five seconds. In the double pause program, the force application was maintained on the sensor for five seconds and released off the sensor for five seconds. The single pause plot in Figure 4.2 shows that even with sustained pressure, the hysteresis is still apparent. The double pause plot in Figure 4.3 seemingly eliminates the irregular hysteresis behavior, but puts too many requirements on the sensor for it to function effectively.

Though these particular results only pertain to the V3 sensor design, the results are similar for all sensor version up until V4. The hysteresis in this elastomer and copper pad configuration of the sensor are difficult to rectify. The double pause scenario provides enough time for the sensor to equilibrate and negate the effect of hysteresis. However, this time requirement between force applications constrains the sensor too much for it to be effective. The V5 sensor design has yet to undergo such testing and is the subject of future exploration.

4.0.2 Hall-Effect Integrated Sensors

From the magnet selection test, it was determined that the 10mm PCB with A1 Hall-effect sensors and 3 magnets was the most sensitive of all tested configurations. The resulting data from the circular test path showed that this configuration produced the largest change in sensor response of all other configurations. This configuration has the largest data range in the absence of an elastomer casing. This means that it will likely have the largest data range after molding in Vytaflex 20. Though the sensor detected the magnet changing polarity multiple times during the test path, because the sensor behaves linearly even around this transition point, this behavior was disregarded.

Figure 4.4 shows the resulting plot of the circular path of 3 magnets over a 10mm A1 Hall-effect sensor array. The plot shows a repeating series of small, medium, and large spikes in data values. Every series of spikes corresponds a circular trajectory at a specific radius and Z offset from the sensor surface. The large spikes in data correspond to a circular

path with a 3mm radius. Though the data points for the 3mm radius path approach the saturation value, it is highly unlikely that the elastomeric sensor will ever shear the magnet close to 3mm without damaging the elastomer first. The data values fall below the nominal 2048 because the magnetic flux is negative. However, this observation has no bearing on the actual sensitivity.

Testing and analysis of the sensor design is the subject of future work. However, certain conclusions were made about the fabrication process for the current version of the sensor. The sensor was thinner than previously examined designs, which is favorable for footwear-integrated sensing applications. However, precise placement of the magnet proved to be difficult. Additional fixturing of the sensor PCB in the curing elastomer was also required.

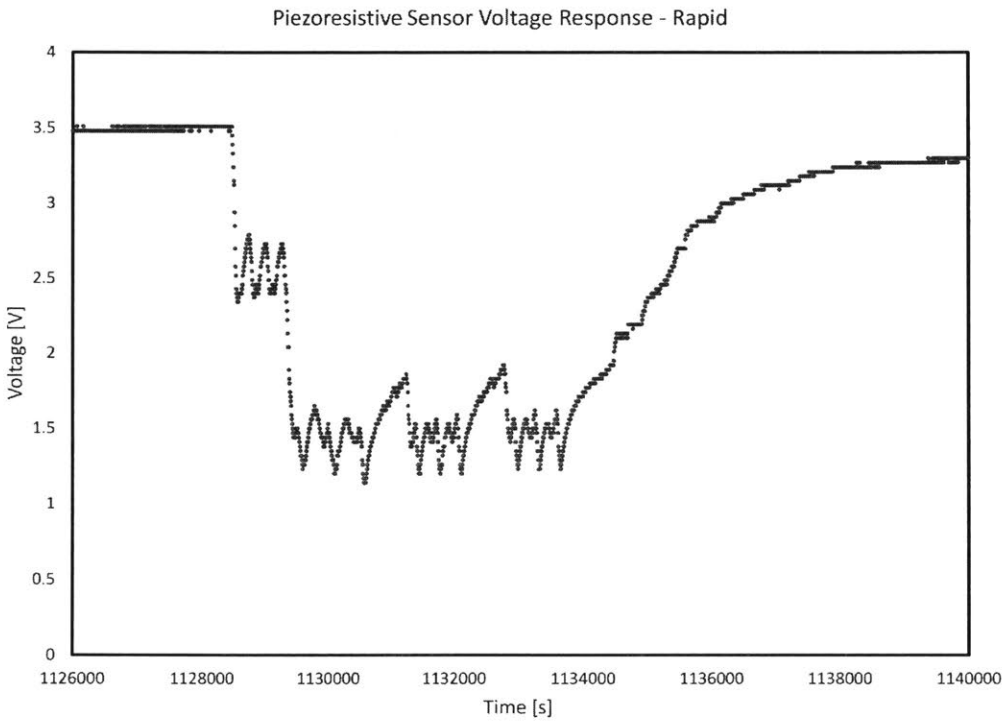

Figure 4.1: Piezoresistive Sensor V3 Voltage Response - Rapid. The graph shown displays the voltage response of a Vytaflex 60/carbon black sensor to a preprogrammed operation controlling force application. The program involved repeated application of three rapid bursts of a lower magnitude force followed by three rapid bursts of a higher magnitude force. This cycle was repeated a total of three times and then ended. The data collection continued until the sensor voltage equilibrated close to the original voltage. After the first cycle, the sensor data for the smaller magnitude bursts were not able to capture the original voltage values due to hysteresis.

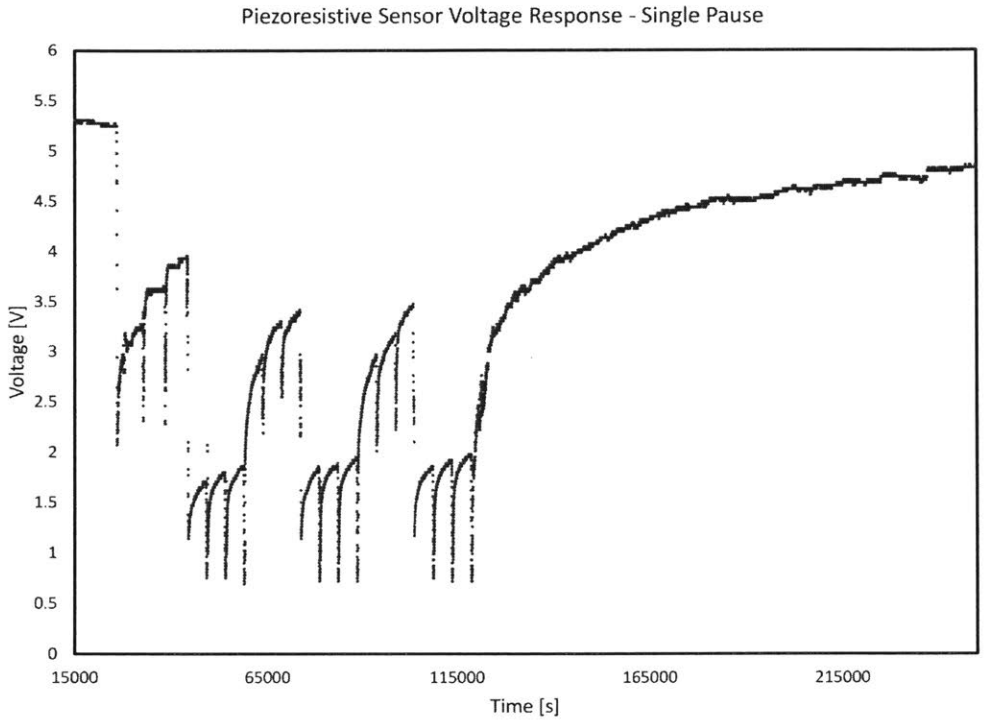

Figure 4.2: Piezoresistive Sensor V3 Voltage Response - Single Pause. The graph shown displays the voltage response of a Vytaflex 60/carbon black sensor to a preprogrammed operation controlling force application. The program involved repeated application of three five-second bursts of a lower magnitude force followed by three five-second bursts of a higher magnitude force. This cycle was repeated a total of three times and then ended. The data collection continued until the sensor voltage equilibrated close to the original voltage. After the first cycle, the sensor data for the smaller magnitude bursts were not able to capture the original voltage values due to hysteresis.

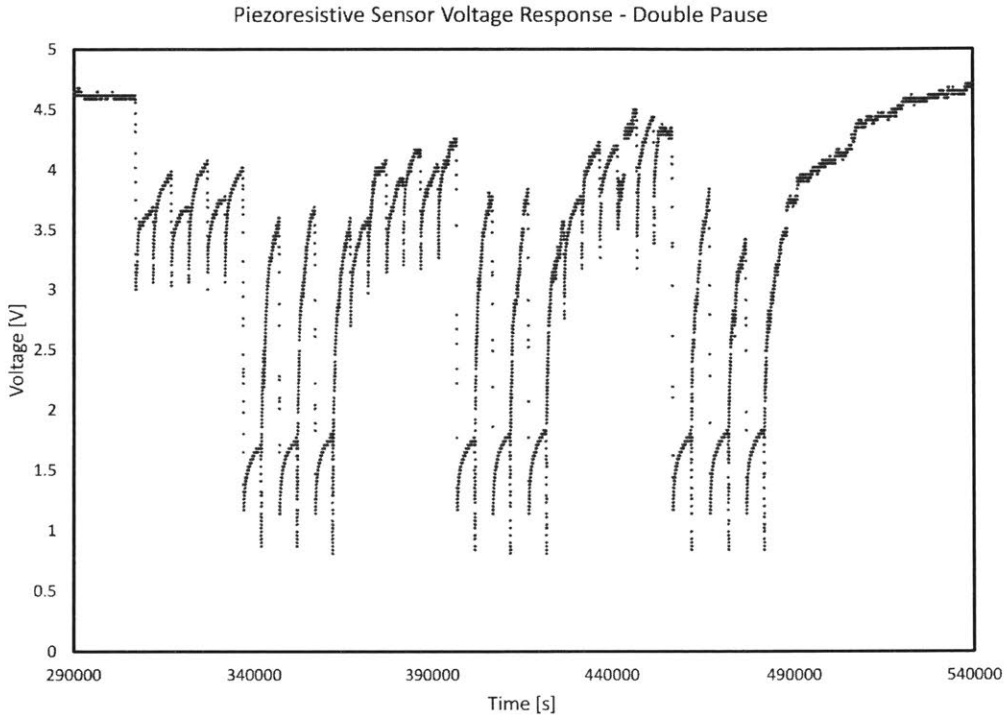

Figure 4.3: Piezoresistive Sensor V3 Voltage Response - Double Pause. The graph shown displays the voltage response of a Vytaflex 60/carbon black sensor to a preprogrammed operation controlling force application. The program involved repeated application of three five-second bursts of a lower magnitude force followed by three sustained bursts of a higher magnitude force. Each burst is followed by a five-second rest period. This cycle was repeated a total of three times and then ended. The data collection continued until the sensor voltage equilibrated close to the original voltage.

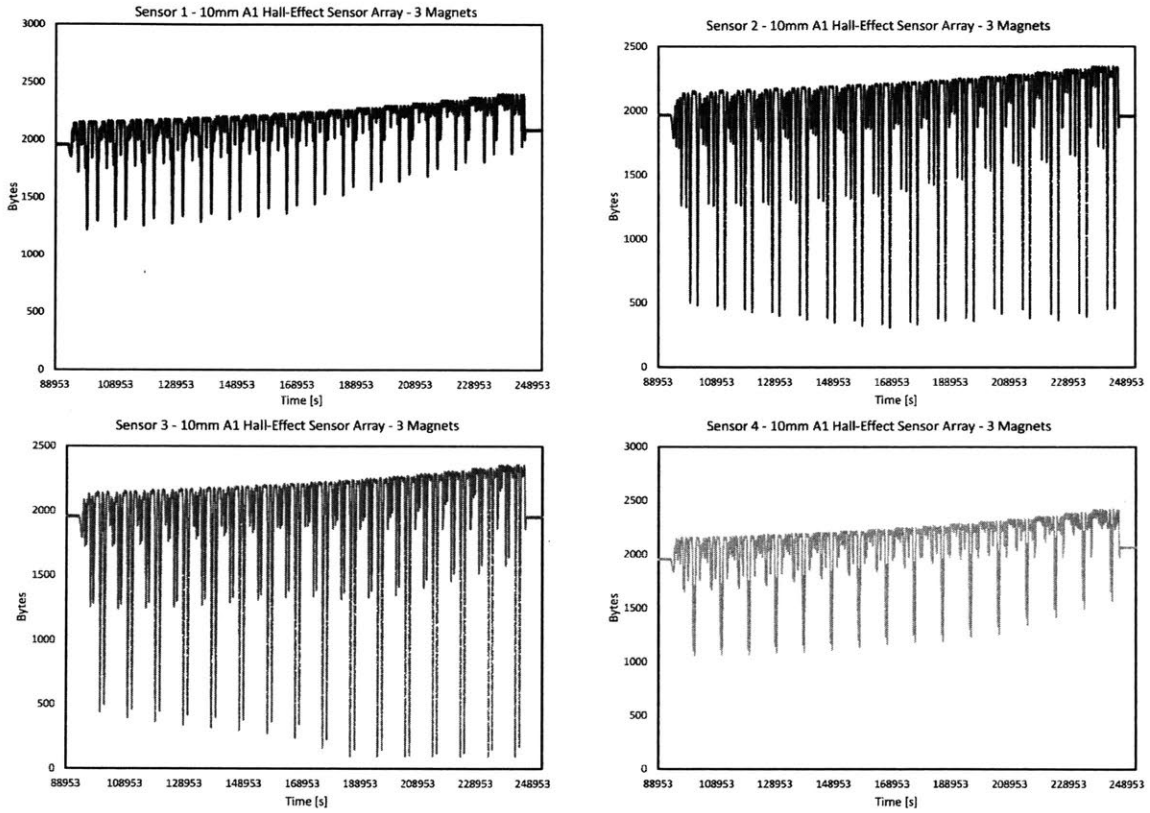

Figure 4.4: 10mm A1 Hall-Effect Sensor Array - Sensor 1-4. The small, medium, and large spikes in sensor data correspond to a circular path with a set radius. Every cycle of repeating spikes corresponds to a different Z offset of the magnet off the sensor surface.

Chapter 5

Conclusions and Future Work

5.1 Conclusion

Based on signal response data for the piezoresistive sensor designs, the hysteresis of the elastomer must be dealt with in order for this method to work effectively. Though the hysteresis behavior for the double pause operation is relatively minor in comparison to the other tested operations, the usage requirement is too restrictive for the sensor to be used effectively in real-world applications. Additionally, the applied force during testing was much lower in magnitude than what the sensor would see in actual operation. Thus, the sensor's signal would saturate if used in its current state. This sensor cannot function based solely on its mechanical properties. In other words, the sensor signal would need computational assistance to interpret the applied forces.

For the Hall-effect integrated sensor design, the overall method shows promise. Preliminary testing of the magnet with the PCB shows that the design is sensitive enough to detect minute magnet movement when cased in elastomer. The most promising orientation involves using three small NdFeB magnets placed approximately 3mm above the surface of the 10mm A1 Hall-effect sensor array. The final sensor is approximately 15mm in thickness, which is thinner than other Hall-effect plantar sensor designs that were investigated. The fabrication procedure needs further development before definitive results concerning the sensor's overall

potential can be ascertained.

5.2 Future Applications for Force Sensing Smart Shoes

The mitigation of hysteresis behavior and saturation of the V1-V4 piezoresistive elastomer sensor designs can be investigated in future work. The V5 sensor will also be investigated in closer detail. Future sensor designs based on these findings will endure further testing and refinement as necessary.

Future work on the Hall-effect integrated sensor design will involve fabrication procedure refinement and force testing. Specifically, the fabrication procedure will need to simplify the magnet placement method as well as shorten fabrication time (ignoring the elastomer cure time). The procedure will also need to include a step for integrating shielding material. This material will prevent magnetic field noise in the surrounding environment from disturbing the sensor readings. For future sensor force testing, the fully fabricated sensor will be attached the spindle of the CNC miniature mill. A force sensor will then be fixed onto the table of the mill. The mill spindle will move according to prescribed depths to compress the Hall-effect integrated sensor onto the force sensor. The force sensor data is then captured and plotted using NI LabVIEW. The corresponding Hall-effect sensor data is collected contemporaneously. In future work, these two sensor data sets will be compared and analyzed to determine the relationship between applied force and magnet shift. This data will then be used to back-calculate the normal and shear force application on the Hall-effect tactile sensor in real time. This will serve as a proof of concept for the use of the sensor as a potential plantar sensing technique. The force testing will also help to refine the design and determine if the sensor can be fabricated to even thinner dimensions.

Chapter 6

References

[1] Abdul Razak, A. H., Zayegh, A., Begg, R. K., and Wahab, Y., 2012, "Foot Plantar Pressure Measurement System: A Review," Sensors (Switzerland), 12(7), pp. 9884–9912.

[2] Anker, J. N., Hall, W. P., Lyandres, O., Shah, N. C., Zhao, J., and Van Duyne, R. P., 2008, "Biosensing with Plasmonic Nanosensors," Nat. Mater., 7(6), pp. 442–453.

[3] Boer, G. De, Raske, N., Wang, H., Ghajari, M., Culmer, P., and Hewson, R., 2017, "Design Optimisation of a Magnetic Field Based Soft Tactile Sensor," Sensors, 17(2539).

[4] Boulton, A. J. M., Hardisty, C. A., Betts, R. P., Franks, C. I., Worth, R. C., Ward, J. D., and Duckworth, T., 1983, "Dynamic Foot Pressure and Other Studies as Diagnostic and Management Aids in Diabetic Neuropathy," Diabetes Care, 6(1), p. 26 LP–33.

[5] Canavese, G., Stassi, S., Fallauto, C., Corbellini, S., Cauda, V., Camarchia, V., Pirola, M., and Pirri, C. F., 2014, "Piezoresistive Flexible Composite for Robotic Tactile Applications," Sensors Actuators, A Phys., 208, pp. 1–9.

[6] Chuah, M. Y. (Michael), 2018, "Design Principles of Multi–Axis , Large Magnitude Force Sensors Based on Stress Fields for Use in Human and Robotic Locomotion," MIT.

[7] Chuah, M. Y. (Michael), Estrada, M., and Kim, S., 2012, "Composite Force Sensing Foot Utilizing Volumetric Displacement of a Hyperelastic Polymer," IEEE Int. Conf. Intell. Robot. Syst., (September), pp. 1963–1969.

[8] Downey, A., and Laflamme, S., 2017, "Experimental Wind Tunnel Study of a Smart Sensing Skin for Condition Evaluation of a Wind Turbine Blade PhD Project View Project," (October).

[9] Engel, J., Chen, J., and Liu, C., 2003, "Development of Polyimide Flexible Tactile Sensor Skin," J. Micromech. Microeng., 13, pp. 359–366.

[10] Gomez, S. C., Vona, M., and Kanoulas, D., 2015, "A Three-Toe Biped Foot with Hall-Effect Sensing," IEEE Int. Conf. Intell. Robot. Syst., 2015–Decem, pp. 360–365.

[11] Guo, C., Wu, C., Wang, B., and Liu, H., 2017, "A Two-Dimensional Deflection Sensor Based on Force Sensing Resistors," J. Sensors, 2017.

[12] Hennig, E. M., and Sterzing, T., 2009, "Sensitivity Mapping of The Human Foot: Thresholds at 30 Skin Locations," Foot Ankle Int., 30(10), pp. 987–991.

[13] Hidalgo-Lpez, J. A., Oballe-Peinado, ., Castellanos-Ramos, J., Snchez-Durn, J. A., Fernndez-Ramos, R., and Vidal-Verd, F., 2017, "High-Accuracy Readout Electronics for Piezoresistive Tactile Sensors," Sensors, 17(2513).

[14] Johnson, K. O., 2001, "The Roles and Functions of Cutaneous Mechanoreceptors," Curr. Opin. Neurobiol., 11(4), pp. 455–461.

[15] Kappassov, Z., Corrales, J. A., and Perdereau, V., 2015, "Tactile Sensing in Dexterous Robot Hands - Review," Rob. Auton. Syst., 74, pp. 195–220.

[16] Kennedy, P. M., and Inglis, J. T., 2002, "Distribution and Behavior of Glabrous Cutaneous Receptors in the Human Foot Sole," J. Physiol., 583.3(3), pp. 995–1002.

[17] Liang, Q., Zhang, D., Coppola, G., Wang, Y., Wei, S., and Ge, Y., 2014, "Dimensional MEMS/micro Sensor for Force and Moment Sensing: A Review," IEEE Sens. J., 14(8), pp. 2643–2657.

[18] Lobmann, R., Kayser, R., Kasten, G., Kasten, U., Kluge, K., Neumann, W., and Lehnert, H., 2001, "Effects of Preventive Footwear on Foot Pressure as Determined by Pedabarography in Diabetic Patients: A Prospective Study.," Diabet. Med., 18, pp. 314–319.

[19] Manabe, H., Fukumoto, M., and Yagi, T., 2013, "Conductive Rubber Electrodes for Earphone-Based Eye Gesture Input Interface," Proc. 17th Annu. Int. Symp. wearable Comput., pp. 33–39.

[20] Nawata, K., Nishihara, S., Hayashi, I., and Teshima, R., 2005, "Plantar Pressure Distribution during Gait in Athletes with Functional Instability of the Ankle Joint: Preliminary Report," J. Orthop. Sci., 10(3), pp. 298–301.

[21] Papakostas, T. V, Lima, J., and Lowe, M., 2002, "A Barge Area Force Sensor for Smart Skin Applications," pp. 1620–1624.

[22] Piacenza, P., and Sherman, S., 2018, "Data-Driven Super-Resolution on a Tactile Dome," 3(3), pp. 1434–1441.

[23] Pirri, C. F., Stassi, S., Cauda, V., and Canavese, G., 2014, "Flexible Tactile Sensing Based on Piezoresistive Composites: A Review," Sensors (Basel)., 14(3), pp. 5296–5332.

[24] Poupyrev, I., Gong, N.-W., Fukuhara, S., Karagozler, M. E., Schwesig, C., and Robinson, K. E., 2016, "Project Jacquard," Proc. 2016 CHI Conf. Hum. Factors Comput. Syst. - CHI '16, pp. 4216–4227.

[25] Queen, R. M., Mall, N. A., Nunley, J. A., and Chuckpaiwong, B., 2009, "Differences in Plantar Loading between Flat and Normal Feet during Different Athletic Tasks," Gait Posture, 29(4), pp. 582–586.

[26] Rosenbaum, D., and Becker, H.-P., 1997, "Plantar Pressure Distribution Measurements. Technical Background and Clinical Applications," Foot Ankle Surg., 3(1), pp. 1–14.

[27] Roy, D., Wettels, N., and Loeb, G. E., 2013, "Elastomeric Skin Selection for a Fluid-Filled Artificial Fingertip," J. Appl. Polym. Sci., 127(6), pp. 4624–4633.

[28] Studebaker, S., 2017, "Material Modeling and Sensor Characterization for Optimizing Footpad Force Sensing Array," MIT.

[29] Taya, M., Kim, W. J., and Ono, K., 1998, "Piezoresistivity of a Short Fiber/elastomer Matrix Composite," Mech. Mater., 28(1–4), pp. 53–59.

[30] Tiwana, M. I., Redmond, S. J., and Lovell, N. H., 2012, "A Review of Tactile Sensing Technologies with Applications in Biomedical Engineering," Sensors Actuators, A Phys., 179, pp. 17–31.

[31] Wang, F., 2015, "Soft Tactile Sensors for Human-Machine Interaction BT - Handbook of Smart Textiles," X. Tao, ed., Springer Singapore, Singapore, pp. 317–355.

[32] Watanabe, Y., Uemura, S., and Hoshino, S., 2014, "Printed Pressure Sensor Array Sheets Fabricated Using Poly (Amino Acid) -Based Piezoelectric Elements," Jpn. J. Appl. Phys., 15, p. 05HB15.

[33] Woo, M. E., 2013, "Development of a Porous Piezoresistive Material and Its Application to Underwater Pressure Sensors and Tactile Sensors."

[34] Xu, T., Wang, W., Bian, X., Wang, X., Wang, X., Luo, J. K., and Dong, S., 2015, "High Resolution Skin-like Sensor Capable of Sensing and Visualizing Various Sensations and Three Dimensional Shape," Sci. Rep., 5(August 2014), pp. 1–9.

[35] Yoon, S.-W., Park, W.-S., and Lee, J.-W., 2016, "Effects of Body Mass Index on Plantar Pressure and Balance," J. Phys. Ther. Sci., 28(11), pp. 3095–3098.

[36] Yousef, H., Boukallel, M., and Althoefer, K., 2011, "Tactile Sensing for Dexterous in-Hand Manipulation in Robotics - A Review," Sensors Actuators, A Phys., 167(2), pp. 171–187.

[37] Zou, D., Mueller, M. J., and Lott, D. J., 2007, "Effect of Peak Pressure and Pressure Gradient on Subsurface Shear Stresses in the Neuropathic Foot," J. Biomech., 40(4), pp.

883–890.